NASA
Technical
Paper
3237

September 1992

Radiation Dose to Critical Body Organs for October 1989 Proton Event

Lisa C. Simonsen,
William Atwell,
John E. Nealy,
and Francis A. Cucinotta

NASA

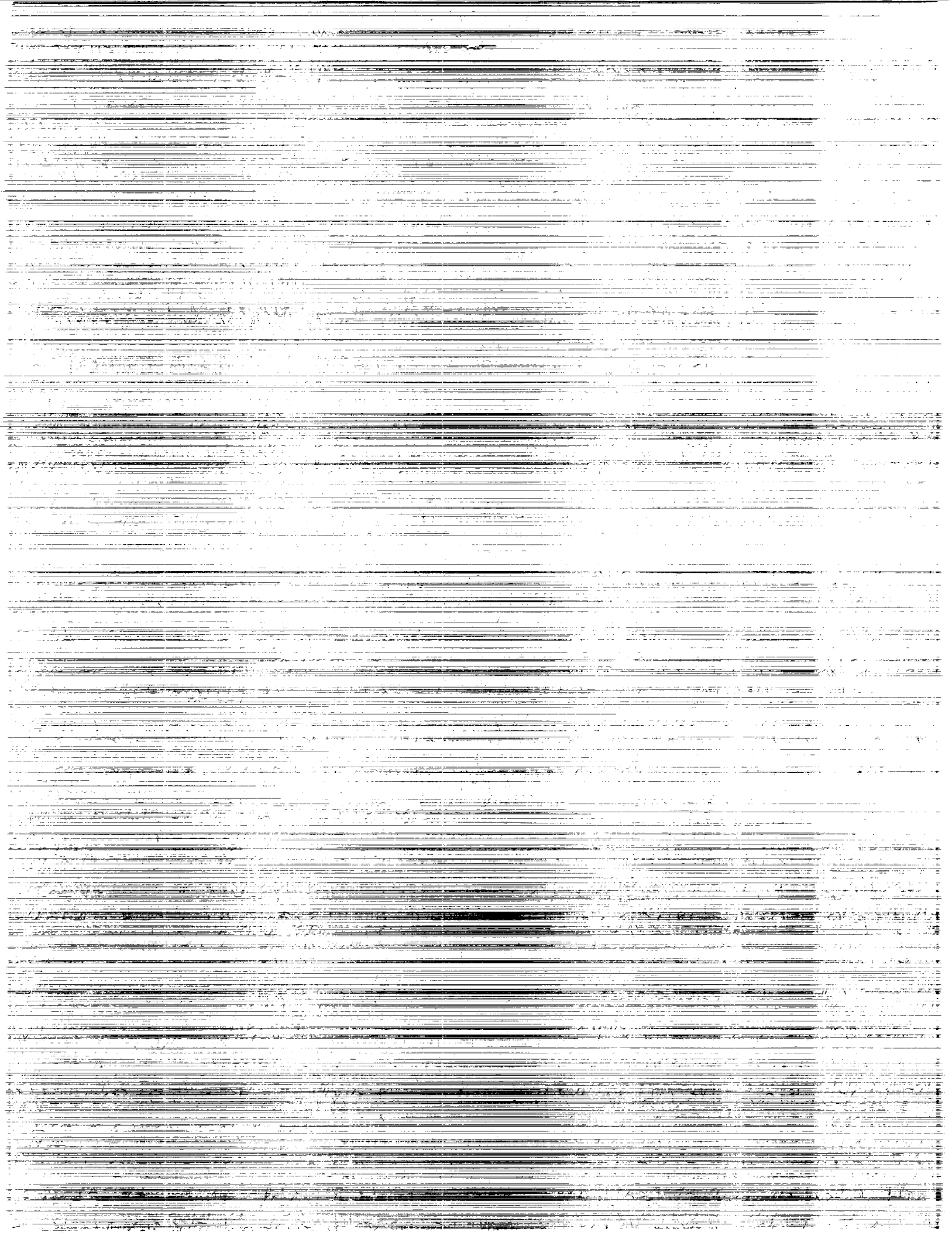

NASA Technical Paper 3237

1992

Radiation Dose to Critical Body Organs for October 1989 Proton Event

Lisa C. Simonsen
Langley Research Center
Hampton, Virginia

William Atwell
Rockwell International
Space Systems Division
Houston, Texas

John E. Nealy
and Francis A. Cucinotta
Langley Research Center
Hampton, Virginia

NASA
National Aeronautics and Space Administration
Office of Management
Scientific and Technical Information Program

Abstract

The Geostationary Operational Environmental Satellite (GOES-7) provides high-quality environmental data about the temporal development and energy characteristics of the protons emitted during a solar particle event. The GOES-7 time history of the hourly averaged integral proton flux for various particle kinetic energies are analyzed for the solar proton event occurring October 19–29, 1989. This event is similar to the August 1972 event that has been widely studied to estimate free-space and planetary radiation-protection requirements. By analyzing the time-history data, the dose rates, which can vary over many orders of magnitude in the early phases of the flare, can be estimated as well as the cumulative dose as a function of time. When basic transport results are coupled with detailed body organ thickness distributions calculated with the Computerized Anatomical Man and Computerized Anatomical Female models, the dose rates and cumulative doses to specific organs can be predicted. With these results, the risks of cancer incidence and mortality are estimated for astronauts in free space protected by various water shield thicknesses.

Introduction

Once outside the Earth's protective magnetosphere, a crew on a lunar or Mars mission will encounter a harsh free-space radiation environment including galactic cosmic rays and solar flare protons. The October 1989 flare is typical of the rarely occurring large flares, while the smaller normally occurring flares are much less hazardous. Galactic cosmic rays (GCR) are also a source of exposure characterized by a much lower but continuous dose rate. The contribution to dose from GCR becomes more important as mission duration increases. This study investigates the high dose rate delivered by a typical large flare that can be mission threatening if crew members are unable to retreat to sufficiently shielded areas. Early or acute effects from such a large dose can include blood count changes, vomiting, and possibly death. In addition, the crew and mission planners must also consider the delayed or late effects of excessive radiation exposure. Several late biological effects to consider are the risk of cancer induction and mortality, the risk of cataract induction, and the risk of infertility. Dose estimates to critical body organs can be estimated by analyzing flare transport and dosimetry calculations in conjunction with anatomical thickness distributions to assess possible health effects.

The potential exposure of critical body organs is evaluated for the 1989 October proton event. Six significant flares that occurred from August to November 1989 have been recorded by the Geostationary Operational Environmental Satellite (GOES-7). GOES-7 is a weather satellite in geostationary orbit above 75°W and is operated by the National Oceanic and Atmospheric Administration (NOAA). The GOES-7 also monitors the temporal development and energy characteristics of protons emitted during solar particle events. Of the six 1989 flares recorded, the flare occurring October 19–29 had the largest free-space dose potential. The high-quality environmental data from GOES-7 allow a more detailed study of the recent flares compared with earlier flare events, such as the widely studied February 1956, November 1960, and August 1972 events. Details on the measurements of flare characteristics of earlier solar cycles (XIX to XXI) have been documented (refs. 1 and 2). Figure 1 compares the proton fluence energy spectra of the four large events. As illustrated, the October 1989 flare is on the order of the large August 1972 event.

The scope of this paper focuses on the time history of the October 1989 proton event. Potential dose rates and cumulative doses are estimated for critical body organs of astronauts protected by varying amounts of shielding. This paper assesses excess lifetime risks of cancer incidence and mortality as well as possible early health effects.

Symbols

D	dose, Gy or cGy
E	energy, MeV
F	integral flux, protons/cm^2-sec-sr
H	dose equivalent, Sv or cSv
J	integral fluence, particles/cm^2
Q	quality factor
R	rigidity

RISK	risk of cancer incidence or mortality per 1000 population
S	stopping power, MeV/cm
t	thickness, cm
x	distance, cm
μ	total nuclear cross section, cm^{-1}
σ	differential interaction cross section, cm^{-1}-MeV^{-1}
ϕ	differental flux, particles/cm^2-sec-MeV

Nomenclature

BFO	blood-forming organ
BRYNTRN	a baryon transport code
CAF	Computerized Anatomical Female
CAM	Computerized Anatomical Man
EVA	extravehicular activity
GCR	galactic cosmic rays
GOES-7	Geostationary Operational Environmental Satellite
Gray	1.0 Gy = 100 rad, 1 cGy = 1 rad
HZE	high charge and energy
ICRP	International Commission on Radiological Protection
ICRU	International Commission on Radiation Units and Measurements
LET	linear energy transfer
LEO	low-Earth orbit
NCRP	National Council on Radiation Protection and Measurement
NOAA	National Oceanic and Atmospheric Administration
Sievert	1.0 Sv = 100 rem, 1 cSv = 1 rem

Radiation Exposure

Currently dose limits are not established for exploratory class missions; however, it is recommended that limits established for low-Earth-orbit operations be used as guidelines (ref. 3). These limits are established by the National Council on Radiation Protection and Measurement (NCRP) and include dose limits for the skin, ocular lens, and vital organs as shown in table 1 (ref. 3). For high-energy radiation from solar proton flares, the dose delivered to the vital organs is important with regard to latent carcinogenic effects and is often referred to as the blood-forming-organ (BFO) dose. The doses incurred during a proton flare will include a high linear energy transfer (LET) component through the production of nuclear reaction products in tissue. The biological effects of these HZE (high charge and energy) particles are not well understood and lead to uncertainty in risk estimates (refs. 3 and 4). Dose-equivalent limits for carcinogenic and mutagenic effects are established for short-term (30-day) exposures, annual exposures, and total career exposures. These values are listed in table 1. The short-term (30-day) exposures are important when considering solar flare events because of their high dose rate. It is believed that by adhering to the short-term limits, nonstochastic late effects as well as acute effects of the bone marrow, ocular lens, and skin can be held to acceptable levels (ref. 3).

Table 1. Ionizing Radiation-Exposure Limits for Space Station *Freedom* Astronauts

[Data from NCRP-98 (ref. 3)]

Exposure interval	Dose equivalent, cSv		
	Blood-forming organ	Ocular lens	Skin
30 day	25	100	150
Annual	50	200	300
Career	100–400[a]	400	600

[a]Varies with gender and age at initial exposure, see table 2.

Total career exposure limits for the BFO are determined by the gender of the individual and the age at the time of initial exposure (table 2). To estimate exposure limits for ages other than those shown in table 2, an approximate linear relationship (ref. 3) exists as follows:

For males . . . Limit = 2 + 0.075 (Age - 30) Sv

For females . . . Limit = 2 + 0.075 (Age - 38) Sv

The recommended career limits are based on a 3-percent lifetime excess risk of fatal cancer from induced tumors. An excess 3-percent lifetime risk can be compared with the "naturally" occurring risk of fatal cancer, which is approximately 18 percent for males and 15 percent for females (ref. 3).

Table 2. Career Dose-Equivalent Limits for a Lifetime Excess Risk of Fatal Cancer of 3 Percent as a Function of Age at Exposure

[Data from NCRP-98 (ref. 3)]

	BFO dose-equivalent, cSv, limit for first exposure at an age of—			
Gender	25 yr	35 yr	45 yr	50 yr
Male	150	250	325	400
Female	100	175	250	300

Acute effects, such as radiation sickness or death, are manifested by direct energy deposition. If a 1.5 to 2.0 Gy whole-body dose were incurred in a short time period, an individual would have a 50-percent chance of prodromal vomiting within 2 days. Vomiting, which is especially serious for a helmeted individual, has an estimated effective threshold of 1 Gy. If a 3.2 to 5.4 Gy whole-body dose were incurred in a short time period, an individual with minimal to supportive medical care would have a 50-percent chance of death within 20 to 40 days. (See ref. 3.) The estimated effective threshold for mortality is 1.5 Gy.

Of the ocular tissues, the lens of the eye is the most susceptible to radiation-induced damage. Damage to other ocular tissues, which have estimated threshold doses on the order of 10 to 20 Gy, seems unlikely to exhibit tissue damage of clinical significance during space travel (ref. 3). The opacification of the lens or formation of cataracts has a significantly lower threshold dose, with a single dose of approximately 1 to 2 Gy causing minimal stationary opacities (ref. 3).

Large solar proton events have the potential to deliver significant doses to the skin. One effect of such an acute exposure is erythema and moist desquamation, or reddening of the skin (similar to a severe sunburn) and blister formation (second-degree burns). A dose of approximately 6 Gy causes erythema in 50 percent of individuals, while the more serious moist desquamation requires a dose of approximately 20 Gy for a 50-percent response. Late effects to the skin, which can appear months to years later and can occur without evidence of early acute reaction, can include vascular damage, dermal fibrosis, and atrophy of the epidermis and dermis (ref. 3).

Fertility, although not a life-threatening effect, can be a major concern to crew members. Sensitivity to radiation-induced sterility varies with age. Women over 40 years old are more susceptible to radiation-induced menopause than younger women. Doses greater than approximately 1 Gy to the ovaries can produce transient sterility for a few months, while doses less than 1 Gy are unlikely to have any long-term effects on sterility (ref. 3). Smaller doses are required for transient male sterility. A single 0.15 Gy acute dose to the testes significantly lowers the sperm count of 40 percent of males within approximately 2 months. Doses of 0.3 Gy to 0.5 Gy can result in decreased sperm count and temporary sterility lasting between 10 to 20 months, with doses up to 4 Gy causing temporary sterility or infertility for up to 30 months (ref. 2).

Computerized Anatomical Models

Estimates of specific dose and dose equivalent to the skin, ocular lens, and blood-forming organs are calculated through use of the Computerized Anatomical Man (CAM) model (ref. 5). These doses are compared with the frequently used slab-dose estimates to determine the quantitative differences resulting from the use of the detailed model. When detailed body geometry is not considered, the BFO dose is usually computed as the slab dose at a 5-cm depth in tissue. The skin dose can be approximated by a 0.1-cm-depth dose, and the ocular lens dose can be approximated by a 0.3-cm-depth dose. Typically to further simplify dose and shielding estimates, a 0-cm-depth dose for both the skin and the ocular lens can be conservatively used.

The CAM model used to calculate the shielding influence of the human body geometry is based on the fiftieth percentile United States Air Force male in the standing position. Each tissue thickness distribution surrounding a given point within the body is calculated with an evenly spaced distribution of 512 rays over a solid angle of 4π. For example, for each of the 512 rays emanating from a specific location in an organ, the equivalent thickness of water traversed based on organ, bone, and other constituent densities encountered before exiting the body are calculated. The Computerized Anatomical Female (CAF) model uses a 0.92 scale factor to the CAM model and incorporates the female reproductive organs (ref. 6).

The thickness distributions derived from the CAM and CAF models (figs. 2 to 9) are used to estimate potential doses from the October 1989 event. The skin, ocular lens, and BFO distributions are plotted in figure 2 as percent thickness less than t versus t. These distributions are used in a manner analogous to a cumulative probability distribution function of the thickness traversed in every direction

about a given point. The skin and BFO distributions are each averages of 33 locations within the human body model, while the ocular lens distribution is approximated by a single reference point. The BFO locations include points within the pelvis, hip, humerus, sternum, femur, fibula, and other areas of bone marrow production.

The doses to various other organs such as the thyroid, lung, esophagus, stomach, intestine, liver, pancreas, kidney, bladder, testes, ovary, uterus, and breast can also be calculated through use of computer-generated thickness distributions. Both the CAM and CAF thyroid distributions are averages of four distributions calculated at separate reference points within the thyroid. The directionality dependence of the thickness distribution is maintained during the averaging process, where for each of the 512 directions, the average thickness in the particular direction is determined. The resulting average thicknesses are then arranged into the percent thickness less than t versus t form for illustration. Figure 3 shows the distribution of each of the selected points for the CAM thyroid, with the dashed line representing the average of the distributions. The average CAM and CAF thyroid distributions are compared in figure 4. With the CAM thickness distribution greater at most depths, the effects of the CAF 0.92 scale factor are apparent. All other internal organ distributions, with the exception of the stomach, right lung, and breast, are evaluated at a single point. The stomach and right lung distributions represent averages of five locations, while the breast represents an average of four locations. Distributions associated with the digestive system are shown in figure 5. The pancreas and liver distributions are very similar (fig. 6); thus, the predicted doses are expected to be comparable. On the other hand, the dose estimates are expected to be much greater for the testes than for the kidney because of the large differences in their distributions (fig. 7). The CAF distributions for several female organs are included in figures 8 and 9. Potential doses to the various organs can be estimated by using each of these thickness distributions in conjunction with dose-depth curves calculated for the October 1989 event.

Analysis of Flare Data

The time history of the integral proton flux for various particle kinetic energy values is shown in figure 10 for the 10-day period beginning at 00:00 UTC (Coordinated Universal Time) on October 19, 1989. These data are hourly averaged flux values recorded by the GOES-7 proton monitor (ref. 7). As shown in figure 10, three major pulses of high-energy protons arrived at the satellite during this event. In addition, a strong magnetic disturbance during the first pulse (≈12 hours after the initial flux increase) caused flux levels at all energies shown to increase by factors of 5 or more for 4 to 5 hours.

To use the satellite data in the baryon transport code BRYNTRN (ref. 8) developed at NASA Langley Research Center, the integral fluxes at a given time are interpolated and extrapolated to the code energy grid points according to the usual rigidity parameterization:

$$F = F_0 \exp\left(\frac{-R}{R_0}\right)$$

where F is the integral flux, F_0 and R_0 are curve-fit parameters, and R is the rigidity:

$$R = [E^2 + 2(938.26)E]^{1/2}$$

for energy E in units of MeV. The integral fluxes at the desired grid energies are then numerically differentiated to obtain the differential fluxes required for the transport calculations. This procedure is performed for various time values during the event. These time values are selected to reasonably characterize the temporal flux behavior (i.e., times corresponding to maximum and minimum flux values and times intermediate to where the extrema occur). A table listing the integral fluxes at each energy value for the 14 times chosen during the episode (ref. 7) is included in the appendix.

Another useful display of the data that illustrates the time-development of the flare is given in figure 11, which gives the differential fluences at successive times during the event. As shown in figure 11, a large fraction of the proton flux is encountered by day 2 of the data period. For purposes of this analysis, the event is assumed to be over at day 10.

Transport and Dosimetry Calculations

Once the differential fluxes at each time value are obtained from the raw data, the nucleon transport computer code BRYNTRN (ref. 8) is used to predict the propagation and interactions of nucleons through various media. The code uses an algorithm that provides solutions to the Boltzmann equation in the one-dimensional, or "straight ahead," approximation form:

$$\left[\frac{\partial}{\partial x} - \frac{\partial}{\partial E}\, S_j(E) + \mu_j(E)\right]\phi_j(x, E) = \sum_{k>j} \int_E^\infty \sigma_{jk}(E, E')\, \phi_k(x, E')\, dE'$$

where the quantity to be evaluated, $\phi_j(x, E)$, is the flux of particles of type j (protons or neutrons) having energy E at spatial location x. The solution methodology of this integrodifferential equation can be described as a combined analytical-numerical technique (ref. 9). The accuracy of this numerical method has been determined to be within approximately 1 percent of exact benchmark solutions (ref. 10). The data required for solution consist of the stopping power S_j in various media, the macroscopic total nuclear cross sections μ_j, and the differential nuclear interaction cross sections σ_{jk}. The differential cross sections describe the production of type j particles with energy E by type k particles of energy E'. Detailed information on these data base compilations is described in reference 8. Salient features of this code and its implementation are described in references 8, 11, and 12.

Once the particle fluxes are determined, the absorbed dose (in units of Gy) can be computed. The absorbed dose due to energy deposition at a given location by all particles can then be related to biological risk by introducing the quality factor Q, as specified by the International Commission on Radiological Protection (ICRP). (See ref. 13.) Thus, the values of dose equivalent H (in units of Sv) used to specify radiation exposure are computed as follows:

$$H(x) = \sum_j \int_0^\infty Q_j(E)\ S_j(E)\ \phi_j(x, E)\ dE$$

These values can be compared with the radiation-exposure limits of table 1. Using the previous approach, the dose and dose equivalent versus depth in water for each of the 14 time values are calculated from the hourly averaged flux.

For the October 1989 flare analysis, transport calculations and corresponding dose-equivalent evaluations are made for normally incident particles on slabs of water as the attenuating medium. Such an approach necessarily invokes the straight-ahead approximation that has been shown to slightly overestimate the actual exposure for space radiations (ref. 14). Water is selected for all CAM and CAF thicknesses because it provides a good simulation of human tissue with regard to ionizing radiation transport. For shield thicknesses, the dose calculations for water can often provide good estimates for equivalent thicknesses of organic and organic-composite materials. The shield density thickness (g/cm^2) requirements for aluminum and other higher atomic numbered materials are greater. The October 1989 flare spectrum is relatively deficient in high-energy particles; therefore, for the shield thicknesses considered in this study (0.5, 2.0, 5.0, and 10.0 g/cm^2), the estimated doses behind effective shield thicknesses of aluminum are approximately 25 to 30 percent greater than the estimated doses behind corresponding water shield thicknesses (ref. 15).

The dose-depth functions shown in figure 12 compare the present 10-day time-integrated results computed with the ICRP-26 quality factors with corresponding calculations using the integral fluence rigidity function of reference 7 for both ICRP-26 and ICRU-40 quality factors (ref. 16). Even more recently, quality factors have been recommended by ICRP-60 (ref. 17). Neither the ICRU-40 nor the ICRP-60 has as yet been accepted by any regulatory body in the United States. The ICRU-40 dose-equivalent calculations are comparable with the ICRP-60 calculations for the October 1989 event. While the change in quality factors from ICRP-26 does not significantly affect the dose equivalents for solar proton flares of this type, larger differences are seen for the contributions to dose equivalent from the HZE particles of GCR. The integral fluence rigidity function reported by NOAA (ref. 7) is

$$J = J_0 \exp\left(\frac{-R}{R_0}\right)$$

with J_0 equal to 1.12×10^{11} particles/cm^2 and $R_0 = 77.4$ MV. The differences due to the two quality factors are relatively small ($\approx$5–10 percent, with larger differences occurring at smaller thickness values). Differences between the fluence rigidity-fit values and the time-integrated values are more prominent, particularly at greater thicknesses (15–30 g/cm^2) for which the present results exceed the functional-fit results by 25 to 50 percent. This difference can be explained by the differences in the time-integrated and fluence-fit spectra shown in figure 13. At energies greater than 100 MeV, the present results exhibit higher particle fluence than the fluence-fit function. The present results fall slightly below the fluence-fit curve for energies between approximately 30 and 70 MeV. These features relate directly to the differences observed in figure 12 over the range of thicknesses considered. Also shown in figure 13 are the differential fluence data points from GOES-7 instruments; these points suggest that the actual fluences are greater at higher energies than those evaluated from the fluence-fit function for this flare event.

Discussion of Results

Potential doses to the various organs can be estimated by using each of the anatomical thickness distributions in conjunction with the dose-depth curves

calculated for the October 1989 event. For each of the 512 rays of the thickness distribution, a directional dose is log linearly interpolated/extrapolated from the dose-depth data. The directional dose is then integrated over a solid angle of 4π to determine the total dose at the target point within the organ. The results consist of the dose and dose-equivalent rates evaluated at specific times during the flare event for various shielding thicknesses. The estimated doses are based on slab geometry shield calculations coupled with the CAM and CAF thickness distributions (figs. 2 to 9). Figures 14(a) and 14(b) depict some of these results with the dose variation between selected times assumed to be logarithmic. The comparison of figures 14(a) and 14(b) with figure 10 indicates that the calculated skin dose rate variation with time is generally similar to the flux variation with time. The thickness values of 0.5, 2.0, 5.0, and 10.0 g/cm^2 of water are selected to depict the variation of dose rate with amount of protection. The effective shielding of an extravehicular activity (EVA) suit and a pressurized rover can be represented by 0.5 and 2.0 g/cm^2, respectively, while a 5.0 g/cm^2 thickness approximately corresponds to an Apollo-like capsule. A larger thickness of 10.0 g/cm^2 can represent the shielding protection of a storm shelter. (A linear thickness (cm) is calculated by dividing the density thickness (g/cm^2) by the density (g/cm^3) of the desired material.)

By integrating the dose rates of figures 14(a) and 14(b), the cumulative skin dose and dose equivalent are evaluated as shown in figures 14(c) and 14(d), respectively. These figures can be used to estimate the crew incurred dose during the entire event, with the assumption of various exposure times behind different slab shielding thicknesses. For the October 1989 flare spectrum, the difference between the dose (Gy) and the dose-equivalent (Sv) values is relatively small. The average quality factors for the October 1989 event, obtained by dividing the estimated dose-equivalent values by dose, are on the order of 1.3 to 1.6. The cumulative dose rate curves indicate the amount of exposure incurred in each of the three main pulses. Most of the dose is accumulated in the first day and a half of the flare episode, with significant additional contributions at approximately day 4 and day 6. Although not investigated here, a fractionated dose typically reduces the overall effects of the radiation exposure. The crew can reduce their overall exposure by remaining in heavily shielded areas during peak dose rate times. Similarly, the dose rates and cumulative doses are shown for the eye and BFO in figures 15 and 16.

The 30-day limits (guidelines) of table 1 are indicated on cumulative dose equivalent versus time figures for the skin, eye, and BFO. To remain below the 150-cSv 30-day limit for the skin, a shielding thickness of approximately 4.4 cm of water is required. To remain below the 100-cSv eye and the 25-cSv BFO 30-day limits, shielding thicknesses of 6.0 and 8.4 cm of water, respectively, are required. For the October flare, the protection of the BFO dictates the selection of a shield thickness of at least 8.4 cm of water to reduce the dose to all three organs below the 30-day limits. This amount is the minimum thickness required for this event and assumes no radiation from other sources, for example, galactic cosmic radiation, man-made nuclear sources, or other flare events. The calculated protection may be strictly applicable to short-duration missions or storm shelter protection requirements.

A comparison of the CAM results can be made with the earlier calculated slab estimates (ref. 15) as shown in table 3. For the slab results, the skin dose has been estimated as the 0-cm-depth dose and the BFO dose is estimated as the 5-cm-depth dose. Characteristically, the more detailed CAM calculations result in 20 to 50 percent lower doses than the corresponding slab calculations, with the degree of reduction dependent on the energetic particle environment spectrum. For the October event, both the CAM BFO and skin doses are approximately 40 to 50 percent lower than the corresponding slab estimates. Thus, the estimated minimum shielding requirement of approximately 12 cm of water based on a 5-cm-depth dose can be reduced to 8.4 cm.

Table 3. Comparison of Slab and CAM Dose-Equivalent Estimates

[Data from ref. 15]

Water shield thickness, g/cm^2	Skin dose equivalent, cSv		BFO dose equivalent, cSv	
	Slab	CAM	Slab	CAM
0.5	2525	1132	205	107
2.0	902	426	142	72
5.0	234	127	78	41
10.0	78	46	35	19

The cumulative dose and dose equivalent were calculated for the other organs of figures 2 through 9. Sample calculations of the male thyroid, male right lung, and female right breast are illustrated in figures 17, 18, and 19. The thyroid and lung are

selected as example calculations because of the greater risk of cancer induction to these specific organs. The dose rate and cumulative dose curves are very similar in nature for all organs considered. Tables 4 to 7 list the cumulative dose and dose equivalent for the other organs protected by various shielding thicknesses. With these values, some of the possible effects of this flare to exposed crew members can be assessed.

Table 4. Cumulative Dose (cGy) Incurred for October 1989 Flare for Various Water Shield Thicknesses Calculated With CAM Model Organ Distributions

Location	Cumulative dose, cGy, for shield thickness of—			
	0.5 cm	2.0 cm	5.0 cm	10.0 cm
Eye	599	253	93	35
Skin	721	298	96	35
BFO	80	55	31	15
Thyroid	361	160	66	26
Right lung	53	40	25	12
Esophagus	207	107	51	21
Stomach	27	21	14	8
Intestine	56	42	25	13
Liver	32	25	16	9
Pancreas	31	24	16	8
Right kidney	41	31	19	10
Bladder	42	28	17	9
Right testicle	150	84	41	17

Table 5. Cumulative Dose Equivalent (cSv) Incurred for October 1989 Flare for Various Water Shield Thicknesses Calculated With CAM Model Organ Distributions

Location	Cumulative dose equivalent, cSv, for shield thickness of—			
	0.5 cm	2.0 cm	5.0 cm	10.0 cm
Eye	914	354	123	46
Skin	1132	426	127	46
BFO	107	72	41	20
Thyroid	538	220	87	34
Right lung	70	53	33	17
Esophagus	297	144	67	28
Stomach	36	28	19	11
Intestine	75	56	34	17
Liver	43	33	22	12
Pancreas	41	32	21	12
Right kidney	54	41	26	14
Bladder	58	38	22	12
Right testicle	210	112	54	23

Table 6. Cumulative Dose (cGy) Incurred for October 1989 Flare for Various Water Shield Thicknesses Calculated With CAF Model Organ Distributions

Location	Cumulative dose, cGy, for shield thickness of—			
	0.5 cm	2.0 cm	5.0 cm	10.0 cm
Breast	242	133	64	26
Right ovary	42	32	20	11
Uterus	39	30	19	10
Thyroid	367	163	67	26
Right lung	59	44	27	13
Stomach	31	24	16	9

Table 7. Cumulative Dose Equivalent (cSv) Incurred for October 1989 Flare for Various Water Shield Thicknesses Calculated With CAF Model Organ Distributions

Location	Cumulative dose equivalent, cSv, for shield thickness of—			
	0.5 cm	2.0 cm	5.0 cm	10.0 cm
Breast	337	178	84	34
Right ovary	55	43	27	14
Uterus	52	40	26	14
Thyroid	547	224	89	35
Right lung	78	59	36	18
Stomach	41	32	21	12

For large solar flare exposures, some early effects (evaluated in terms of Gy) can include the possibility of death, vomiting, or skin irritation. The dose to the BFO, used here to estimate whole-body exposure, is predicted to be between 15 and 80 cGy for 10.0 to 0.5 cm of water shielding, respectively. The risk of death or vomiting is unlikely, with the dose estimates below threshold values for such responses. In most instances, an early response of the skin is also unlikely. However, if a crew member were on extended or frequent EVA's ($\approx$0.5 g/cm^2) during the peak dose rate periods, a skin dose of 450 cGy could be incurred; such a dose would produce erythema in approximately 10 percent of individuals exposed.

Late effects (evaluated in terms of Sv) can include the risk of lens opacification, impairment of fertility, and cancer induction. Late effects can occur a few months to years following exposure. For crew members protected by 2.0 to 5.0 cm of water, a dose to the eye of 350 to 100 cSv is estimated and may cause minimal stationary opacities. However, if the crew member were on extended or frequent EVA's ($\approx$0.5 g/cm^2) during the high dose rate periods, a

dose to the eye of almost 600 cSv (fig. 14(d)) could be possible, thus the risk of some degree of lens opacification would be significantly increased. The male is much more susceptible to fertility impairment than the female. With the estimated dose to the ovaries between 14 cSv and 55 cSv, the female is unlikely to have any long-term effects on fertility. However, for the shielding thicknesses examined, the estimated dose to a male testicle is between 23 cSv and 210 cSv. With these doses, the male is likely to have a decreased sperm count with temporary sterility lasting between 10 to 20 months. The risk of cancer induction and mortality is examined in the following section.

The potential dose equivalents estimated for the October 1989 event (tables 5 and 7) can be compared with several organ doses predicted for the August 1972 event as shown in table 8. In general,

Table 8. Predicted Dose Equivalent (cSv) Incurred for August 1972 Flare for Various Water Shield Thicknesses Calculated With CAM and CAF Model Thickness Distributions

Location		Dose equivalent, cSv, for water shield thickness of			
		0.5 cm	2.0 cm	5.0 cm	10.0 cm
CAM model	Skin	1953	879	233	53
	Eye	1673	758	217	51
	BFO	187	110	46	15
	Thyroid	1024	471	144	36
	Right lung	97	64	31	11
	Stomach	36	25	14	6
CAF model	Breast	1054	371	130	35
	Thyroid	1042	480	148	37
	Right lung	112	74	35	12
	Stomach	44	31	16	6

the August 1972 dose-equivalent values are substantially larger than corresponding values for the October 1989 event for smaller shield layers. However, as shield thickness increases, the differences decrease and eventually the trend is reversed with larger doses predicted for the October 1989 event. This behavior can be explained by examining the fluence spectra of figure 1, which shows that the August 1972 proton fluence for energies between approximately 10 and 150 MeV exceeds that of the 1989 flare by as much as a factor of 2 near 60 MeV. Because the range of 60 MeV protons in water is approximately 3 cm, most of the contribution to the dose equivalent is due to primary protons in this intermediate energy range. A proton range of 10 cm corresponds approximately to an energy of 150 MeV, which is approximately where the October 1989 integral fluence exceeds that of the 1972 flare. Accordingly, target points (or organ locations) within the body show more sensitivity to lower and medium energy protons with increasing proximity to the body surface. Thus, differences in the incurred dose equivalents are larger between the two flares for the skin, thyroid, and breast than for the BFO and stomach, which have inherently more shielding. For example, compare the thickness distributions for the CAF model stomach (50-percent thickness greater than 10 cm, fig. 9) and the breast (50-percent thickness less than 3 cm, fig. 8).

Risk Assessment

The lifetime excess risk of cancer incidence and mortality can be estimated with the doses predicted for the various organs. The risk analysis presented here is based on the approach described by the National Council on Radiation Protection and Measurement (ref. 3). The risk of cancer incidence is estimated by the NCRP using radioepidemiological tables developed by the National Institutes of Health (NIH) ad hoc working group (ref. 18). Sufficient information on which to base age and gender-related risk of cancer from radiation exposure was found for the lung, breast, esophagus, stomach, colon, liver, pancreas, kidney and bladder, all acute leukemias, and chronic granulocytic leukemia. Risk estimates for "other sites" were derived in a similar manner by using Biological Effects of Ionizing Radiation (BEIR) (ref. 19) risk estimates and the NIH working group approach. The other sites include tumors of the oral cavity, rectum, gallbladder, uterine corpus, uterine cervix, ovary, brain, bone, connective tissue, prostate, and testis. Risk estimates for incidence of melanoma, lymphoma, and Hodgkin's disease are also included. A linear-quadratic model, in which a linear component dominates at low doses and a quadratic component dominates at high doses, was used for all sites except for the breast and thyroid, for which a linear relationship where the effects are assumed proportional to dose was used. The cancer mortality risk coefficients were estimated by the NCRP using data from the National Institutes of Cancer Surveillance, Epidemiology, and End Results (SEER) program.[1] Many assumptions, constraints, and sources of uncertainty are built into the development of radiation risk coefficients; however, the risk

[1] National Cancer Institute Monogram 57 Report: *Surveillance, Epidemiology and End Results: Incidence and Mortality Data, 1973–1977.* (NIH publ. no. 81-2330.)

projections are based on the best estimates available at the time and are considered to be conservative for space radiation exposure (ref. 3). A discussion of the studies and their shortcomings used to interpret radiation-induced cancer data is included in chapter 5 of reference 3.

Tables of predicted excess lifetime cancer incidence and mortality among 1000 persons are presented in reference 1 for either acute (>5 cGy/day) or protracted (<5 cGy/day) radiation exposures. The tables include projected risks for men and women exposed to ionizing radiation at ages 25, 35, 45, and 55. Lifetime cancer risks for dose exposures other than those listed in the NCRP tables (D_{table}) can be easily estimated for the new dose D of interest. The new risks (RISK) for an acute exposure are calculated with the linear-quadratic relationship

$$\text{RISK} = \frac{\text{RISK}_{\text{table}}\,[D(1 + D/1.16)]}{D_{\text{table}}(1 + D_{\text{table}}/1.16)}$$

for all sites except the breast and thyroid where the linear relationship

$$\text{RISK} = \text{RISK}_{\text{table}}(D/D_{\text{table}})$$

is used. The dose D is in units of Gy, and 1.16 Gy represents the point at which the squared dose contribution is assumed to equal the linear dose contribution. An acute exposure is assumed by the NCRP to be an exposure of greater than 5 cGy/day. The risks presented by NCRP are predicted for exposure to sparsely ionizing radiation such as x or gamma rays. Due to the higher LET with quality factors greater than 1 for the October 1989 spectrum, the dose-equivalent values (cSv) are used to estimate risk instead of dose (cGy) values for the late carcinogenic effect.

The October 1989 event delivers an acute dose equivalent, defined here as greater than 5 cSv/day, to the organs for the various shielding thicknesses. The instantaneous dose-equivalent rates evaluated as a function of time during the course of the flare are used to compute corresponding dose incurred over a 1-day interval. Figures 20 and 21 illustrate the daily dose-equivalent variation for the CAM BFO and stomach distributions, respectively, as obtained by performing the 24-hour running time integration of the corresponding dose rate functions (fig. 16(b) for the BFO and similar data for the stomach). Each dose-equivalent value in figures 20 and 21 represent, at a given time, the cumulative exposure value over the previous 24 hours. Also indicated are the times during the flare at which the dose equivalents to the BFO and stomach are in excess of 5 cSv. For even 10.0 cm of water protection, the 5 cSv value is exceeded during the initial phase of the flare for both the BFO and the stomach. Based on the 24-hour integral dose for the stomach, which has the lowest cumulative dose equivalent (table 5) of the organs considered, an acute exposure is assumed for the October 1989 flare. The associated risks using this assumption are conservative, because the dose is fractionated (allowing time for repair) and the low dose rate contributions (Dose rate < 5 cGy/day) are assumed to be acute.

Predicted excess cancer incidences and mortalities are presented for the male astronaut exposed to the 1989 event in tables 9 to 12 for various shield thicknesses. The risk of total cancers from the flare as well as the risk of cancer to specific organs are shown. The BFO dose equivalent was used to estimate the risk of all acute leukemia and the risk of chronic granulocytic leukemia as well as the risk to other sites. The intestine dose equivalent was used to estimate the dose equivalent to the colon. Table 13 shows the baseline lifetime expected cancer incidences and deaths per 1000 males by age (ref. 3). From table 9, a 25-year-old male with 0.5 cm of shielding would have a 6.28-percent increased chance of obtaining cancer and a 3.4-percent increased chance of dying from cancer. This value can be compared with his overall expected risk of cancer incidence and mortality from "natural" causes of 34.9 percent and 18.4 percent, respectively, as shown in table 13. For a 35-year-old male astronaut in a moderately shielded spacecraft of 5.0 cm of water, an increased risk of cancer incidence and mortality would be 0.98 percent and 0.6 percent, respectively. The use of a storm shelter of 10.0 cm water for the duration of the October event reduces the excess risk of total cancers to less than 1 percent for male astronauts of ages greater than 25 years old.

The overall risk of cancer to females appears greater because of a greater female sensitivity to radiation-induced cancers of the breast and thyroid. The estimated lifetime risk of excess cancer for the female breast and thyroid is shown in table 14 for exposure to the October 1989 flare. For a lightly shielded spacecraft, a 25-year-old female has a greater than 5-percent increased risk of breast cancer. These values can be compared with the baseline lifetime expected cancer incidences and deaths shown in table 15 (ref. 3), where a 25-year-old female has a baseline incidence risk of close to 10 percent. Overall, the projected risks presented in tables 9 to 14 can be used to assess some of the late effects that an exposure to such an event can cause.

Table 9. Predicted Lifetime Risk of Excess Cancer Incidence and Mortality Among 1000 Males for October 1989 Flare With a Water Shield Thickness of 0.5 cm

Type of cancer	Excess risk of lifetime cancers per 1000 males first exposed at age, yr—							
	25		35		45		55	
	Incidence	Mortality	Incidence	Mortality	Incidence	Mortality	Incidence	Mortality
Thyroid	13.45	2.15	8.61	1.61	5.92	1.08	3.23	0.54
Lung	10.44	8.27	7.03	5.58	5.06	4.03	3.72	2.89
Esophagus	6.81	5.84	2.92	2.92	1.95	1.95	2.92	1.95
Stomach	2.30	1.61	1.17	0.83	0.74	0.52	0.69	0.52
Colon	5.00	2.61	2.27	1.25	1.25	0.68	1.25	0.68
Liver	2.50	2.39	0.81	0.81	0.38	0.38	0.22	0.22
Pancreas	1.63	1.53	0.77	0.72	0.46	0.46	0.51	0.46
Kidney and bladder	2.33	0.75	1.28	0.45	0.83	0.30	0.60	0.23
All acute leukemia	2.84	2.46	3.03	2.65	3.41	3.03	3.60	3.03
Chronic granulocytic leukemia	1.51	0.95	1.70	0.95	1.70	0.95	1.70	0.95
All other cancers	14.01	5.49	6.25	2.46	3.41	1.33	2.65	1.14
Total cancer	62.84	34.05	35.84	20.23	25.11	14.70	21.10	12.61

Table 10. Predicted Lifetime Risk of Excess Cancer Incidence and Mortality Among 1000 Males for October 1989 Flare With a Water Shield Thickness of 2.0 cm

Type of cancer	Excess risk of lifetime cancers per 1000 males first exposed at age, yr —							
	25		35		45		55	
	Incidence	Mortality	Incidence	Mortality	Incidence	Mortality	Incidence	Mortality
Thyroid	5.50	0.88	3.52	0.66	2.42	0.44	1.32	0.22
Lung	7.18	5.69	4.83	3.84	3.48	2.77	2.56	1.99
Esophagus	2.08	1.78	0.89	0.89	0.59	0.59	0.89	0.59
Stomach	1.70	1.18	0.86	0.61	0.54	0.38	0.51	0.38
Colon	3.36	1.76	1.53	0.84	0.84	0.46	0.84	0.46
Liver	1.80	1.72	0.59	0.59	0.27	0.27	0.16	0.16
Pancreas	1.20	1.13	0.56	0.53	0.34	0.34	0.38	0.34
Kidney and bladder	1.54	0.50	0.84	0.30	0.54	0.20	0.40	0.15
All acute leukemia	1.61	1.40	1.72	1.50	1.93	1.72	2.04	1.72
Chronic granulocytic leukemia	0.86	0.54	0.97	0.54	0.97	0.54	0.97	0.54
All other cancers	7.95	3.12	3.55	1.40	1.93	0.75	1.50	0.64
Total cancer	34.77	19.68	19.86	11.69	13.87	8.47	11.56	7.19

Table 11. Predicted Lifetime Risk of Excess Cancer Incidence and Mortality Among 1000 Males for October 1989 Flare With a Water Shield Thickness of 5.0 cm

Type of cancer	Excess risk of lifetime cancers per 1000 males first exposed at age, yr—							
	25		35		45		55	
	Incidence	Mortality	Incidence	Mortality	Incidence	Mortality	Incidence	Mortality
Thyroid	2.17	0.35	1.39	0.26	0.96	0.17	0.52	0.09
Lung	3.94	3.12	2.65	2.11	1.91	1.52	1.40	1.09
Esophagus	0.68	0.58	0.29	0.29	0.19	0.19	0.29	0.19
Stomach	1.08	0.75	0.55	0.39	0.35	0.24	0.33	0.24
Colon	1.78	0.93	0.81	0.45	0.45	0.24	0.45	0.24
Liver	1.11	1.06	0.36	0.36	0.17	0.17	0.10	0.10
Pancreas	0.73	0.69	0.34	0.32	0.21	0.21	0.23	0.21
Kidney and bladder	0.86	0.28	0.47	0.17	0.30	0.11	0.22	0.08
All acute leukemia	0.77	0.66	0.82	0.72	0.92	0.82	0.97	0.82
Chronic granulocytic leukemia	0.41	0.26	0.46	0.26	0.46	0.26	0.46	0.26
All other cancers	3.78	1.48	1.69	0.66	0.92	0.36	0.72	0.31
Total cancer	17.31	10.16	9.83	5.97	6.83	4.29	5.68	3.63

Table 12. Predicted Lifetime Risk of Excess Cancer Incidence and Mortality Among 1000 Males for October 1989 Flare With a Water Shield Thickness of 10.0 cm

Type of cancer	Excess risk of lifetime cancers per 1000 males first exposed at age, yr—							
	25		35		45		55	
	Incidence	Mortality	Incidence	Mortality	Incidence	Mortality	Incidence	Mortality
Thyroid	0.85	0.14	0.54	0.10	0.37	0.07	0.20	0.03
Lung	1.81	1.44	1.22	0.97	0.88	0.70	0.65	0.50
Esophagus	0.22	0.19	0.10	0.10	0.06	0.06	0.10	0.06
Stomach	0.59	0.41	0.30	0.21	0.19	0.13	0.18	0.13
Colon	0.79	0.41	0.36	0.20	0.20	0.11	0.20	0.11
Liver	0.56	0.54	0.18	0.18	0.09	0.09	0.05	0.05
Pancreas	0.39	0.37	0.18	0.17	0.11	0.11	0.12	0.11
Kidney and bladder	0.42	0.14	0.23	0.08	0.15	0.05	0.11	0.04
All acute leukemia	0.32	0.28	0.35	0.30	0.39	0.35	0.41	0.35
Chronic granulocytic leukemia	0.17	0.11	0.19	0.11	0.19	0.11	0.19	0.11
All other cancers	1.60	0.63	0.71	0.28	0.39	0.15	0.30	0.13
Total cancer	7.73	4.64	4.37	2.70	3.02	1.93	2.51	1.62

Table 13. Baseline Expected Cancer Incidences and Mortalities per 1000 Male Population by Age

[Data from NCRP-98 (ref. 3)]

Type of cancer	Expected cancer risks per 1000 males by age, yr—							
	25		35		45		55	
	Incidence	Mortality	Incidence	Mortality	Incidence	Mortality	Incidence	Mortality
Thyroid	1.97	0.31	1.73	0.28	1.43	0.23	1.11	0.18
Lung	72.22	57.07	73.63	58.19	74.78	59.10	72.58	57.36
Esophagus	5.36	4.82	5.47	4.91	5.56	4.99	5.35	4.81
Stomach	12.87	9.00	13.09	9.16	13.28	9.29	13.28	9.29
Colon	35.35	18.86	35.94	19.17	36.57	19.51	37.28	19.88
Liver	2.82	2.73	2.85	2.76	2.89	2.80	2.85	2.76
Pancreas	10.91	10.13	11.11	10.32	11.32	10.51	11.31	10.50
Kidney and bladder	32.67	10.19	33.16	10.34	33.50	10.44	33.24	10.37
All acute leukemia	5.15	4.47	5.05	4.39	4.98	4.32	4.92	4.27
Chronic granulocytic leukemia	1.58	0.96	1.53	0.93	1.48	0.90	1.46	0.89
All other cancers	168.25	66.22	168.51	66.33	169.38	66.67	170.16	66.97
Total cancer	349.15	184.77	352.09	186.78	355.16	188.76	353.53	187.27

Table 14. Predicted Lifetime Risk of Excess Cancer Incidences and Mortalities Among 1000 Females for October 1989 Flare

Type of cancer	Water shield thickness, cm	Excess risk of lifetime cancers per 1000 females first exposed at age, yr—							
		25		35		45		55	
		Incidence	Mortality	Incidence	Mortality	Incidence	Mortality	Incidence	Mortality
Thyroid	0.5	42.12	3.83	30.09	2.74	21.88	2.19	14.77	1.64
	2.0	17.25	1.57	12.32	1.12	8.96	0.90	6.05	0.62
	5.0	6.85	0.62	4.90	0.44	3.56	0.36	2.40	0.27
	10.0	2.70	0.25	1.93	0.18	1.40	0.14	0.95	0.11
Breast	0.5	105.14	33.36	64.70	20.56	11.46	3.71	5.73	1.68
	2.0	55.54	17.62	34.18	10.86	6.05	1.96	3.03	0.89
	5.0	26.21	8.32	16.13	5.12	2.86	0.92	1.43	0.42
	10.0	10.61	3.37	6.53	2.07	1.16	0.37	0.58	0.17

Table 15. Baseline Lifetime Expected Cancer Incidences and Mortalities per 1000 Female Population

[Data from NCRP-98 (ref. 3)]

Type of cancer	Age, yr	Risk of incidence	Risk of mortality
Thyroid	25	4.74	0.43
	35	3.88	0.35
	45	2.99	0.27
	55	2.20	0.20
Breast	25	96.12	30.52
	35	95.26	30.25
	45	88.97	28.25
	55	75.13	23.85

Concluding Remarks

With future exploratory class and long-duration missions outside of the Earth's magnetosphere, radiation exposure to crew members is likely to be greater than previously experienced. Thus, crew members should be aware of their risks of both short- and long-term health effects. The capability to determine the doses incurred to the skin, eye, and BFO through use of computerized anatomical models allows a more accurate prediction of the radiation exposure compared with the more conservative 0-cm- and 5-cm-depth slab doses. In addition to the skin, eye, and BFO in which current "guidelines" are established, each organ exhibits its own radiosensitivity based on cancer induction and mortality that is reflected in its corresponding risk coefficients. The ability to predict the dose incurred to the various other organs through use of detailed thickness distributions is important when considering the effects of radiation; for example, the lung and the breast appear to be two of the most sensitive organs. The thyroid also exhibits greater cancer risks due to both its relatively light body self-shielding and its greater radiosensitivity.

Currently, space radiation-exposure limits are established for LEO operations by the NCRP. The BFO limits are selected to maintain the expected excess lifetime risk of fatal cancer to 3 percent. The BFO dose limits are considered representative of the minimum dose required to produce the 3-percent increased risk. With larger doses anticipated for exploratory missions, regulatory commissions may wish to consider expanding limits (from ocular lens, skin, and BFO) to include specific limits for other organs that exhibit high radiosensitivity (e.g., lung, thyroid, and breast). Including new limits such as these may be especially important if mixed crews including female astronauts are considered for future lunar and Mars missions.

Specific measures can be implemented to minimize astronaut risk due to the exposure from flares such as the October 1989 type in which flux intensities vary by many orders of magnitude over several days. This temporal behavior of the proton flux emphasizes the need for active real-time monitoring of the flux intensity with dosimetric instrumentation capable of measuring dose incurred due to deposition of energy in several spectral regions. Such active dosimeters can indicate those times during the flare period that essential crew maintenance activities can be performed under relatively safe conditions. Additionally, spacesuits or other protective apparel can be designed with shield inserts specifically placed to give added protection to radiosensitive areas with relatively little body self-shielding, such as the male reproductive organs, female breast, thyroid, and bone marrow concentrations close to the body surface (pelvic bones, sternum).

NASA Langley Research Center
Hampton, VA 23681-0001
July 30, 1992

Appendix

Hourly Averaged Integral Fluxes for October 1989 Event

Table A1. Hourly Averaged Integral Fluxes at Selected Times During Data Period Used To Calculate Integral Fluence Time Variation at Each Energy

[Data from ref. 7]

Time		Hourly average integral fluxes (protons/cm^2-sec-sr) for $E' > E$, MeV						
Day	Hour	$E > 1$	$E > 5$	$E > 10$	$E > 30$	$E > 50$	$E > 60$	$E > 100$
Oct. 19	06	3.49×10^{0}	3.36×10^{-1}	1.33×10^{-1}	6.50×10^{-2}	4.70×10^{-2}	4.02×10^{-2}	2.09×10^{-2}
Oct. 19	13	2.75×10^{1}	2.36×10^{1}	2.36×10^{1}	2.35×10^{1}	2.24×10^{1}	2.12×10^{1}	1.24×10^{1}
Oct. 19	20	3.10×10^{3}	1.68×10^{3}	1.07×10^{3}	5.60×10^{2}	3.82×10^{2}	3.17×10^{2}	1.69×10^{2}
Oct. 20	04	7.29×10^{3}	4.32×10^{3}	2.41×10^{3}	8.02×10^{2}	4.47×10^{2}	3.50×10^{2}	1.69×10^{2}
Oct. 20	11	2.09×10^{4}	7.66×10^{3}	2.96×10^{3}	6.53×10^{2}	3.17×10^{2}	2.39×10^{2}	1.06×10^{2}
Oct. 20	15	1.86×10^{5}	8.01×10^{4}	3.84×10^{4}	7.15×10^{3}	2.55×10^{3}	1.61×10^{3}	4.93×10^{2}
Oct. 21	01	2.57×10^{4}	7.80×10^{3}	3.51×10^{3}	6.39×10^{2}	2.29×10^{2}	1.43×10^{2}	4.30×10^{1}
Oct. 22	17	1.00×10^{3}	3.81×10^{2}	1.75×10^{2}	2.66×10^{1}	8.44×10^{0}	4.99×10^{0}	1.39×10^{0}
Oct. 22	19	2.59×10^{3}	1.16×10^{3}	9.32×10^{2}	5.46×10^{2}	3.67×10^{2}	2.99×10^{2}	1.54×10^{2}
Oct. 23	04	1.19×10^{4}	4.95×10^{3}	3.61×10^{3}	1.22×10^{3}	5.41×10^{2}	3.58×10^{2}	1.20×10^{2}
Oct. 24	16	1.99×10^{3}	6.30×10^{2}	3.07×10^{2}	6.05×10^{1}	2.18×10^{1}	1.33×10^{1}	3.87×10^{0}
Oct. 25	00	5.08×10^{3}	2.95×10^{3}	2.12×10^{3}	6.96×10^{2}	3.45×10^{2}	2.57×10^{2}	1.17×10^{2}
Oct. 26	16	6.04×10^{3}	6.83×10^{2}	2.56×10^{2}	4.66×10^{1}	1.94×10^{1}	1.36×10^{1}	5.52×10^{0}
Oct. 29	04	7.76×10^{1}	1.62×10^{1}	7.44×10^{0}	1.86×10^{0}	9.32×10^{-1}	7.00×10^{-1}	3.16×10^{-1}

References

1. Foelsche, T.: Specific Solar Flare Events and Associated Radiation Doses. *Space Radiation Effects*, ASTM Special Tech. Publ. No. 363, American Soc. for Testing & Materials, 1963, pp. 1–13.

2. King, Joseph H.: Solar Proton Fluences for 1977–1983 Space Missions. *J. Spacecr. & Rockets,* vol. 11, no. 6, June 1974, pp. 401–408.

3. National Council on Radiation Protection and Measurements: *Guidance on Radiation Received in Space Activities.* NCRP Rep. No. 98, July 31, 1989.

4. Cucinotta, Francis A.; Katz, Robert; Wilson, John W.; Townsend, Lawrence W.; Shinn, Judy; and Hajnal, Ferenc: Biological Effectiveness of High-Energy Protons: Target Fragmentation. *Radiat. Res.*, vol. 127, 1991, pp. 130–137.

5. Billings, M. P.; and Yucker, W. R.: *The Computerized Anatomical Man (CAM) Model.* NASA CR-134043, 1973.

6. Atwell, William; Weyland, Mark D.; and Hardy, Alva C.: Radiation Exposure and Risk Assessment for Critical Female Body Organ. SAE Paper 911352, July 1991.

7. Sauer, Herbert H.; Zwickl, Ronald D.; and Ness, Martha J.: *Summary Data for the Solar Energetic Particle Events of August Through December 1989.* Space Environmental Lab., National Oceanic and Atmospheric Adm., Feb. 21, 1990.

8. Wilson, John W.; Townsend, Lawrence W.; Nealy, John E.; Chun, Sang Y.; Hong, B. S.; Buck, Warren W.; Lamkin, S. L.; Ganapol, Barry D.; Khan, Ferdous; and Cucinotta, Francis A.: *BRYNTRN: A Baryon Transport Model.* NASA TP-2887, 1989.

9. Wilson, John W.: *Analysis of the Theory of High-Energy Ion Transport.* NASA TN D-8381, 1977.

10. Wilson, John W.; and Townsend, Lawrence W.: A Benchmark for Galactic Cosmic-Ray Transport Codes. *Radiat. Res.*, vol. 114, no. 2, May 1988, pp. 201–206.

11. Townsend, L. W.; Wilson, J. W.; Shinn, J. L.; and Curtis, S. B.: Human Exposure to Large Solar Particle Events in Space. Paper presented at the 28th Plenary Meeting of COSPAR (The Hague, The Netherlands), June 25–July 6, 1990.

12. Simonsen, Lisa C.; and Nealy, John E.: *Radiation Protection for Human Missions to the Moon and Mars.* NASA TP-3079, 1991.

13. *Recommendations of the International Commission on Radiological Protection.* ICRP Publ. 26, Pergamon Press, Jan. 17, 1977.

14. Wilson, John W.; Townsend, Lawrence W.; Schimmerling, Walter; Khandelwal, Govind S.; Khan, Ferdous; Nealy, John E.; Cucinotta, Francis A.; Simonsen, Lisa C.; Shinn, Judy L.; and Norbury, John W.: *Transport Methods and Interactions for Space Radiations.* NASA RP-1257, 1991.

15. Simonsen, Lisa C.; Nealy, John E.; Sauer, Herbert H.; and Townsend, Lawrence W.: Solar Flare Protection for Manned Lunar Missions: Analysis of the October 1989 Proton Flare Event. SAE Tech. Paper Ser. 911351, July 1991.

16. *The Quality Factor in Radiation Protection.* ICRU Rep. 40, International Commission on Radiation Units and Measurements, Apr. 4, 1986.

17. *1990 Recommendations of the International Commission on Radiological Protection.* ICRP Publ. 60, International Commission on Radiological Protection, c.1991.

18. National Inst. of Health: *Report of the National Institutes of Health Ad Hoc Working Group To Develop Radioepidemiological Tables.* Rep. No. NIH/PUB-85-2748, Jan. 1985. (Available from NTIS as PB88 208 889/XAB.)

19. Div. of Medical Sciences: *The Effects on Populations of Exposure to Low Levels of Ionizing Radiation.* National Academy of Sciences, National Research Council, 1976.

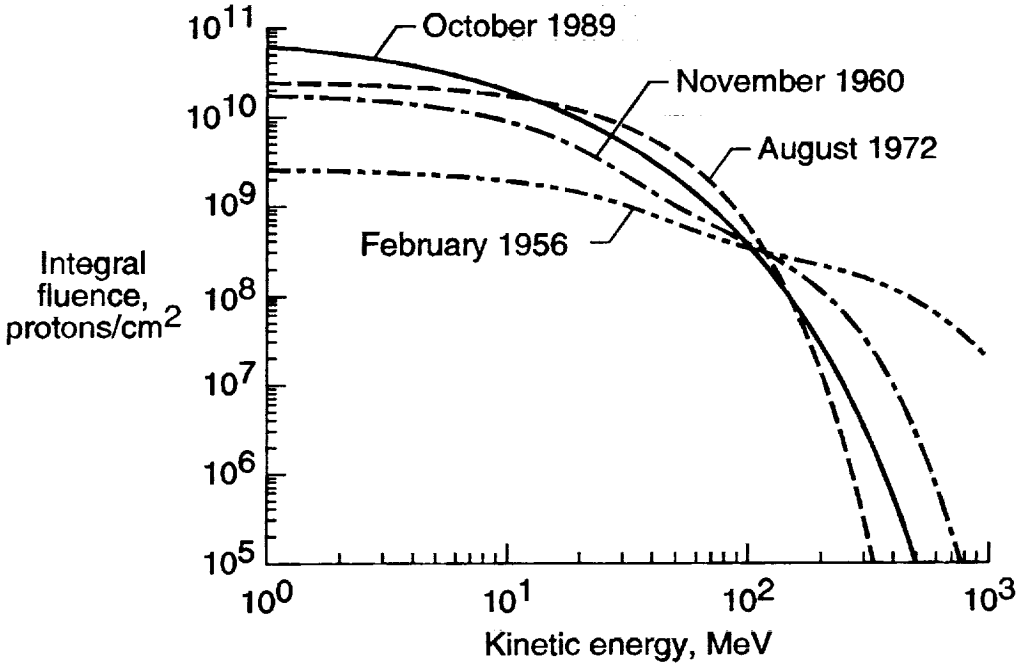

Figure 1. Integral fluence as a function of energy for four large proton flares.

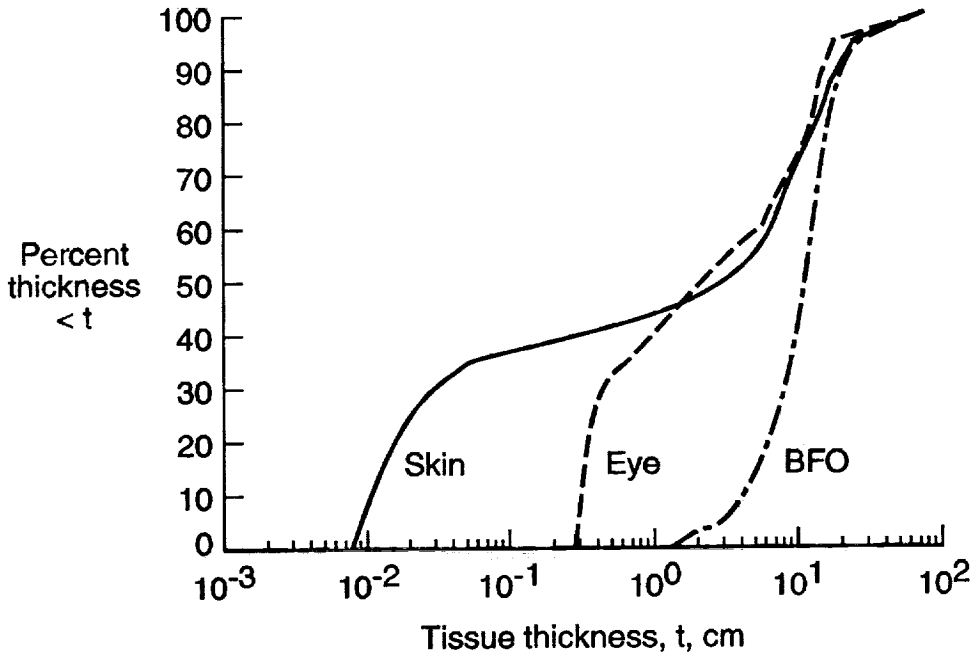

Figure 2. CAM model water thickness distributions for skin, eye, and BFO.

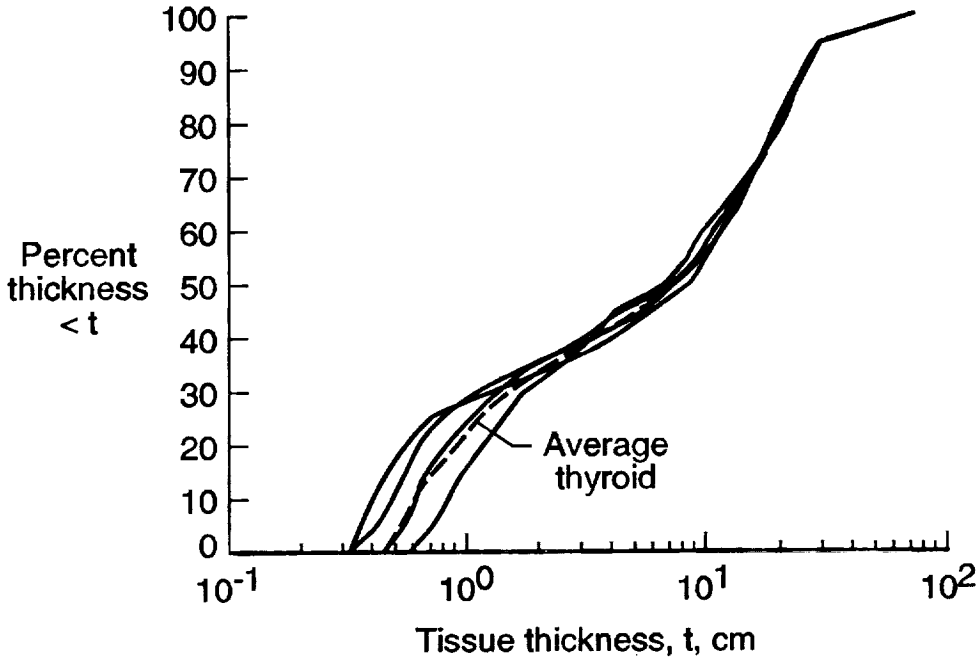

Figure 3. CAM model water thickness distributions for four separate points within the thyroid and directional-averaged thyroid distribution.

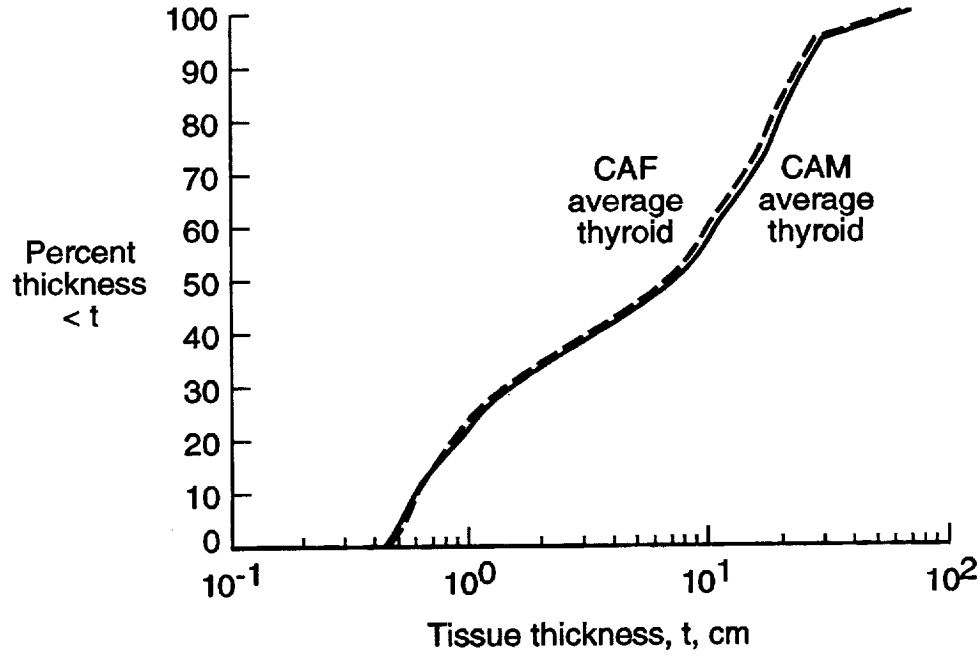

Figure 4. Comparison of CAM and CAF average thyroid water thickness distributions.

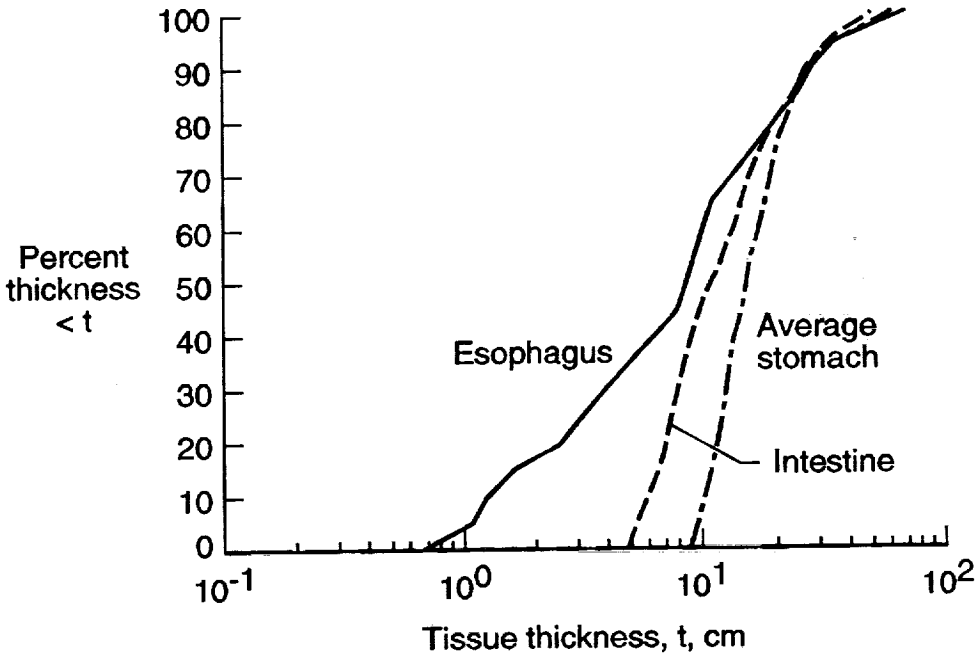

Figure 5. CAM model water thickness distributions for esophagus, intestine, and stomach.

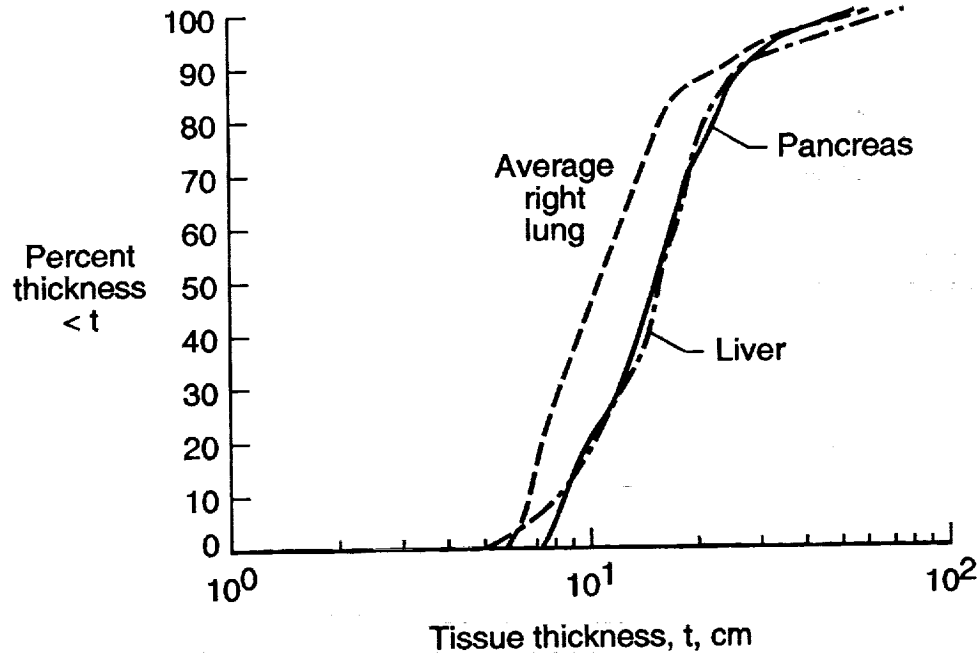

Figure 6. CAM model water thickness distributions for right lung, liver, and pancreas.

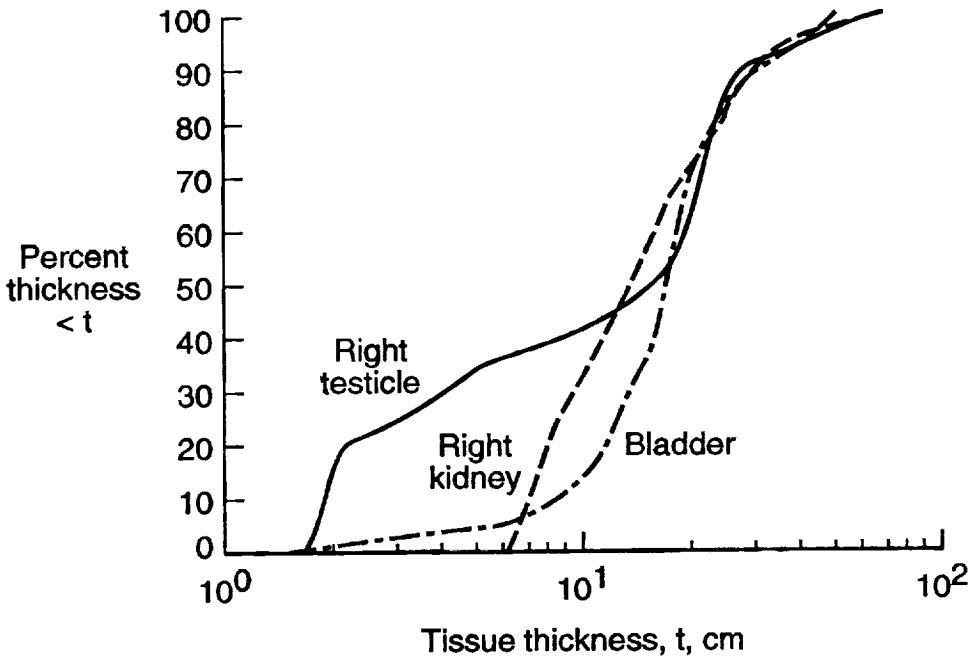

Figure 7. CAM model water thickness distributions for right testicle, right kidney, and bladder.

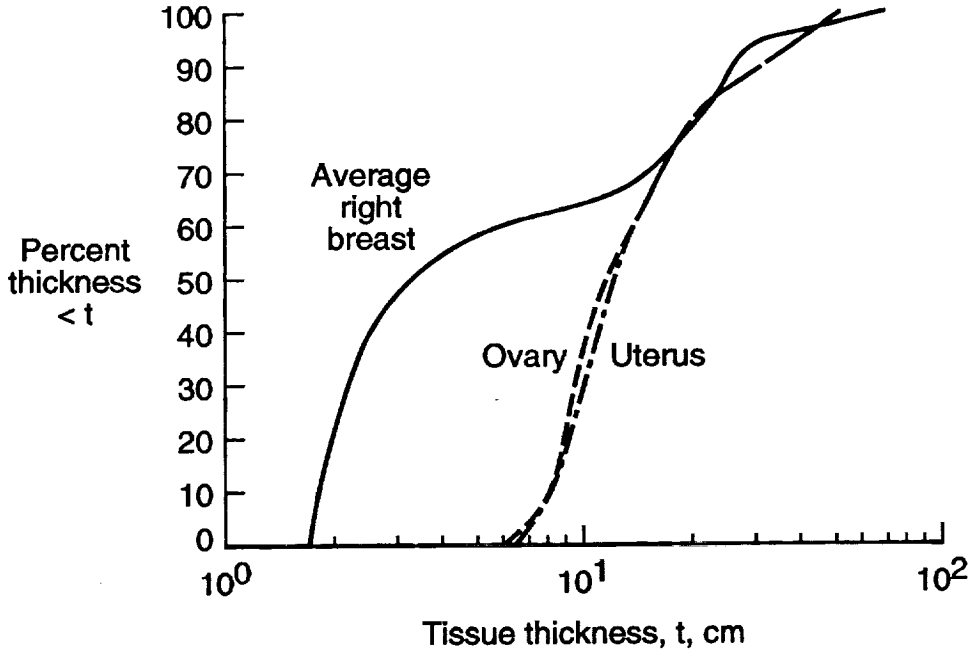

Figure 8. CAF model water thickness distributions for right breast, ovary, and uterus.

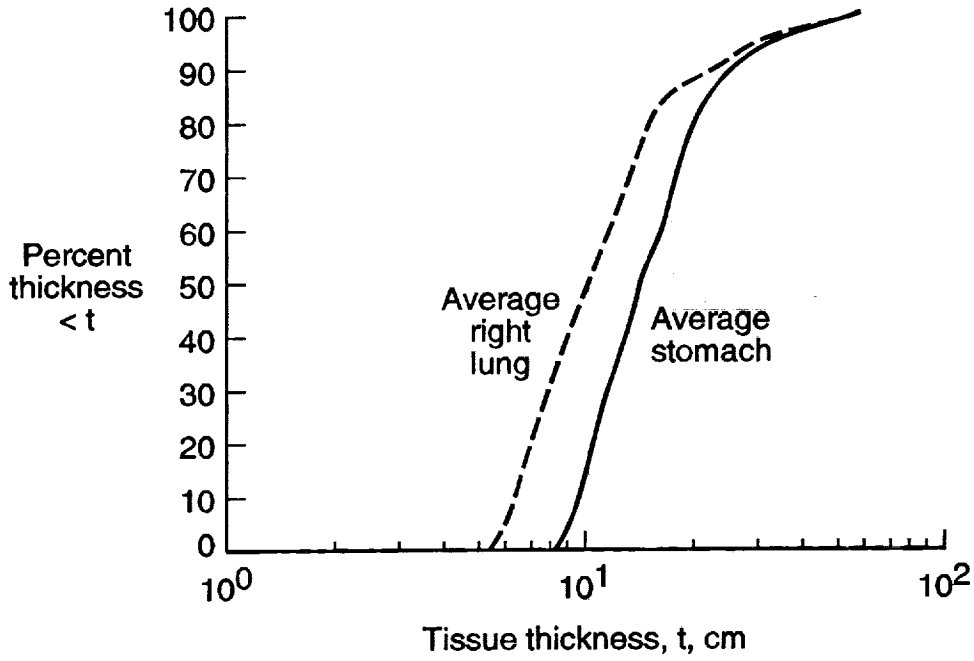

Figure 9. CAF model water thickness distributions for right lung and stomach.

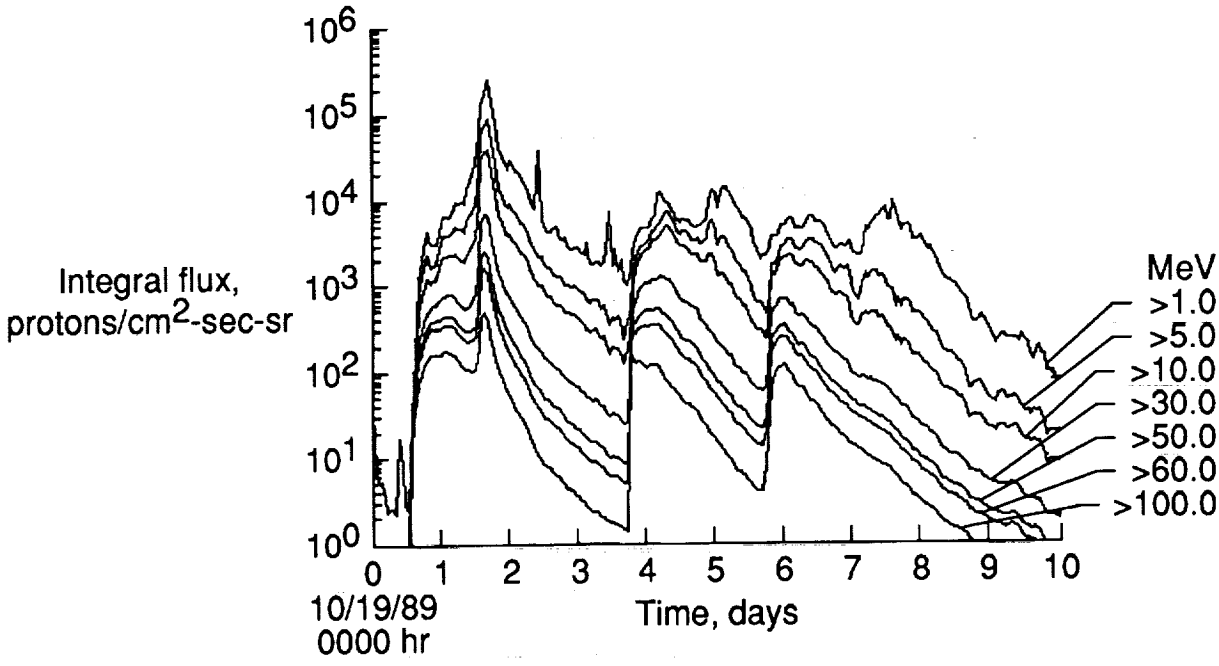

Figure 10. Hourly averaged integral flux history for October 1989 solar flare event. (GOES-7 data from NOAA Space Environment Laboratory, ref. 7.)

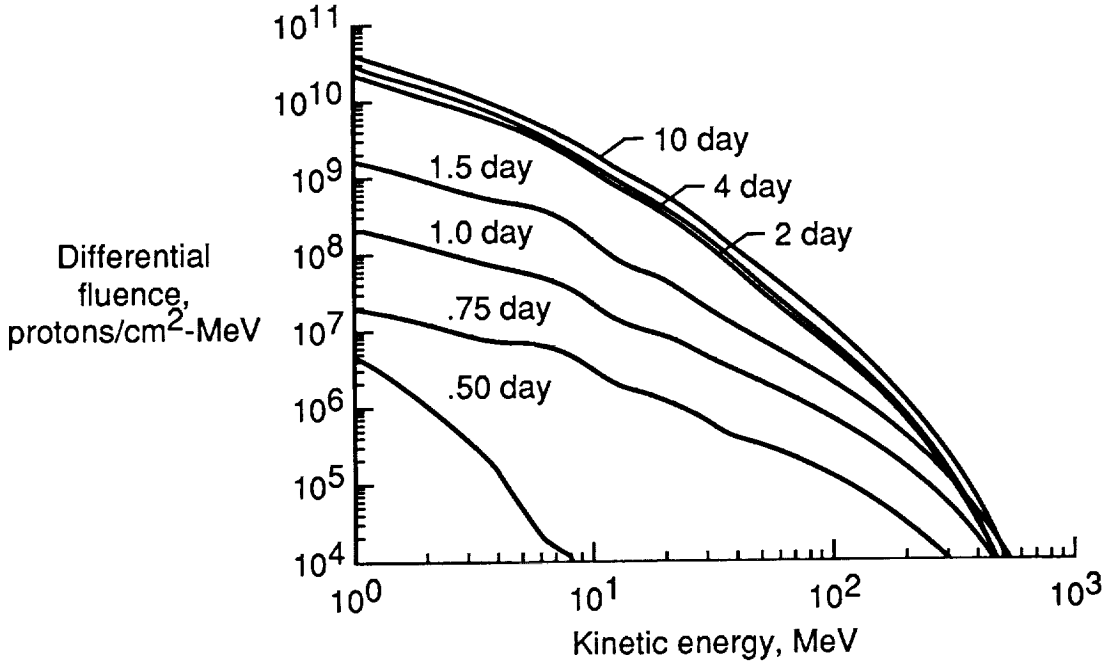

Figure 11. Cumulative differential fluence for October 1989 flare event at selected times.

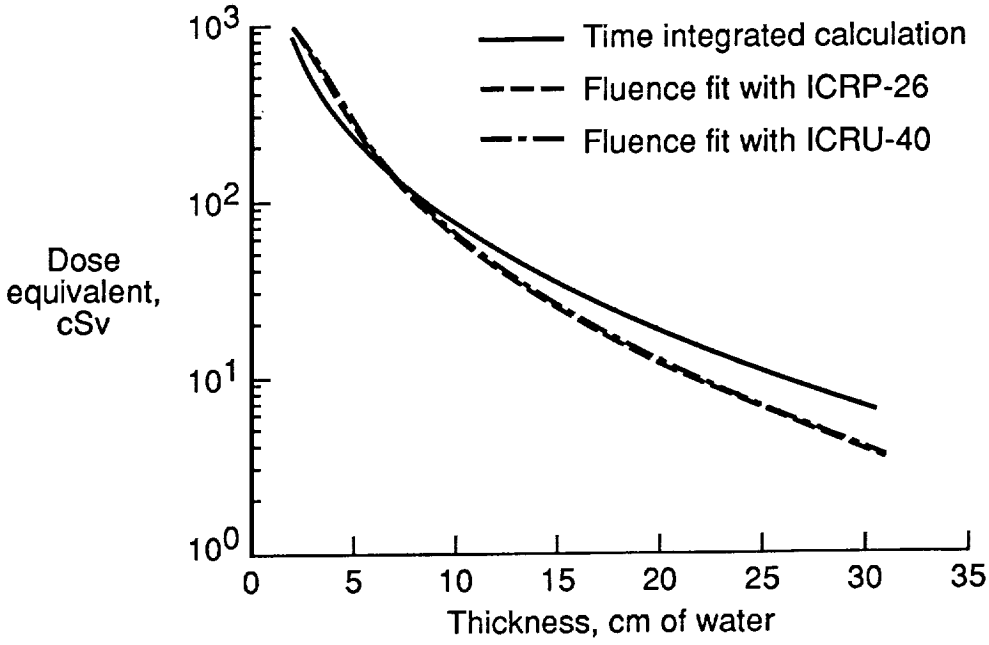

Figure 12. Comparison of dose-depth curves for October 1989 proton event through use of various calculation techniques.

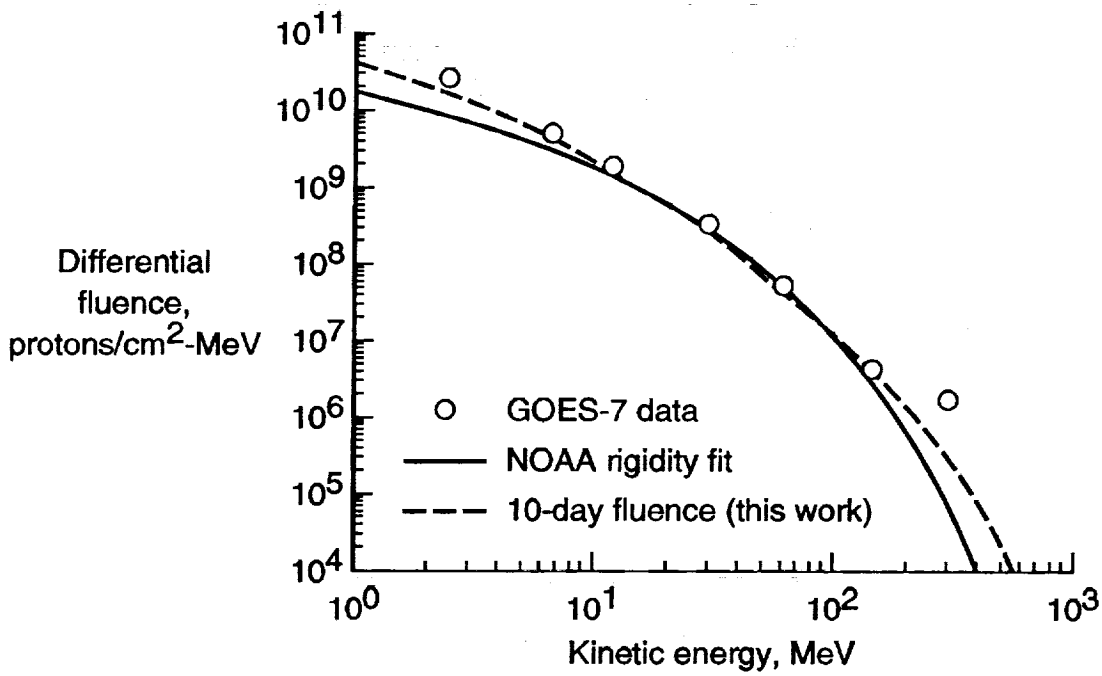

Figure 13. Comparison of differential fluence as a function of energy for the NOAA rigidity fit versus 10-day time-integrated fluence.

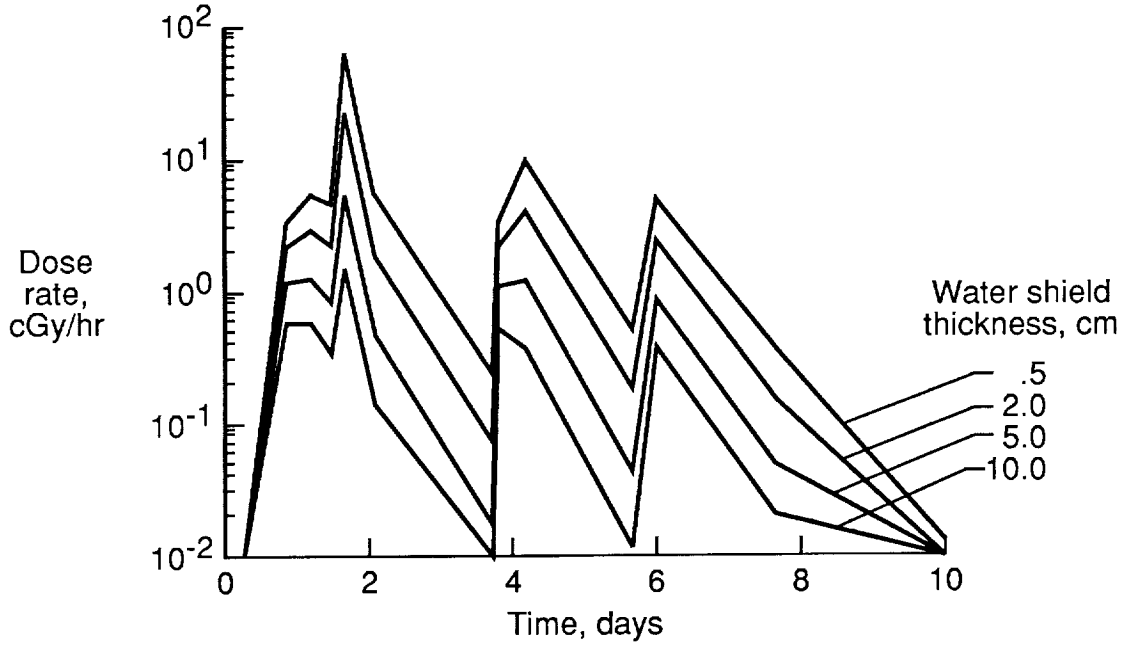

(a) Skin dose rate.

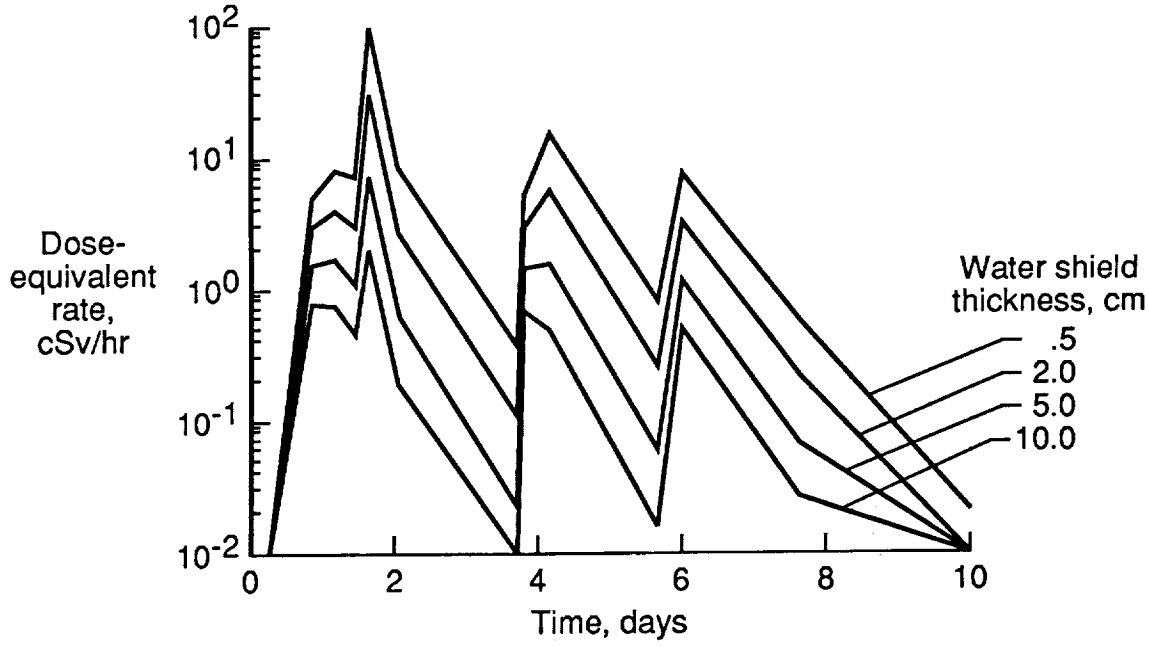

(b) Skin dose-equivalent rate.

Figure 14. Predicted skin dose rate variation and cumulative dose during October 1989 event with 0.5, 2.0, 5.0, and 10.0 cm of water shield thickness.

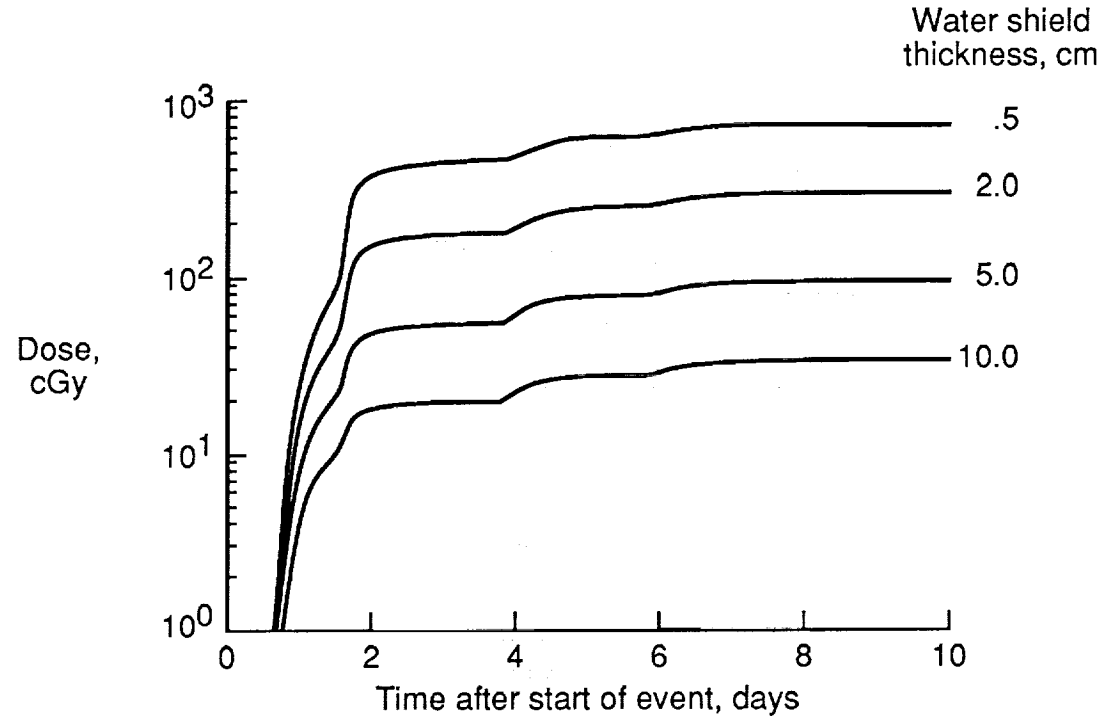

(c) Cumulative skin dose.

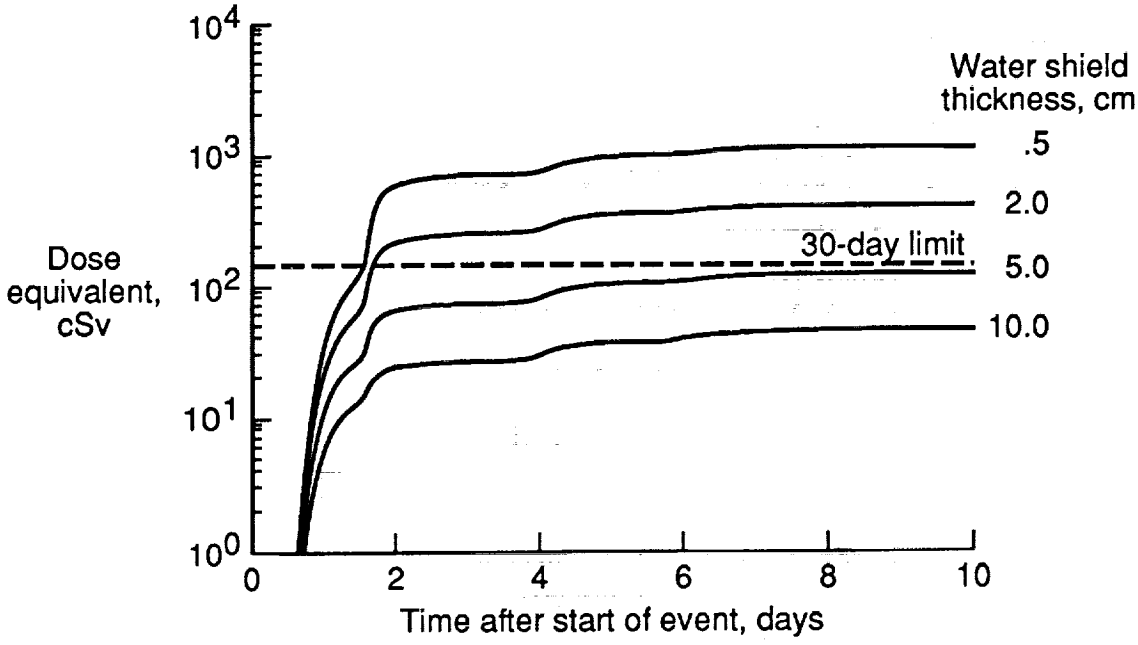

(d) Cumulative skin dose equivalent.

Figure 14. Concluded.

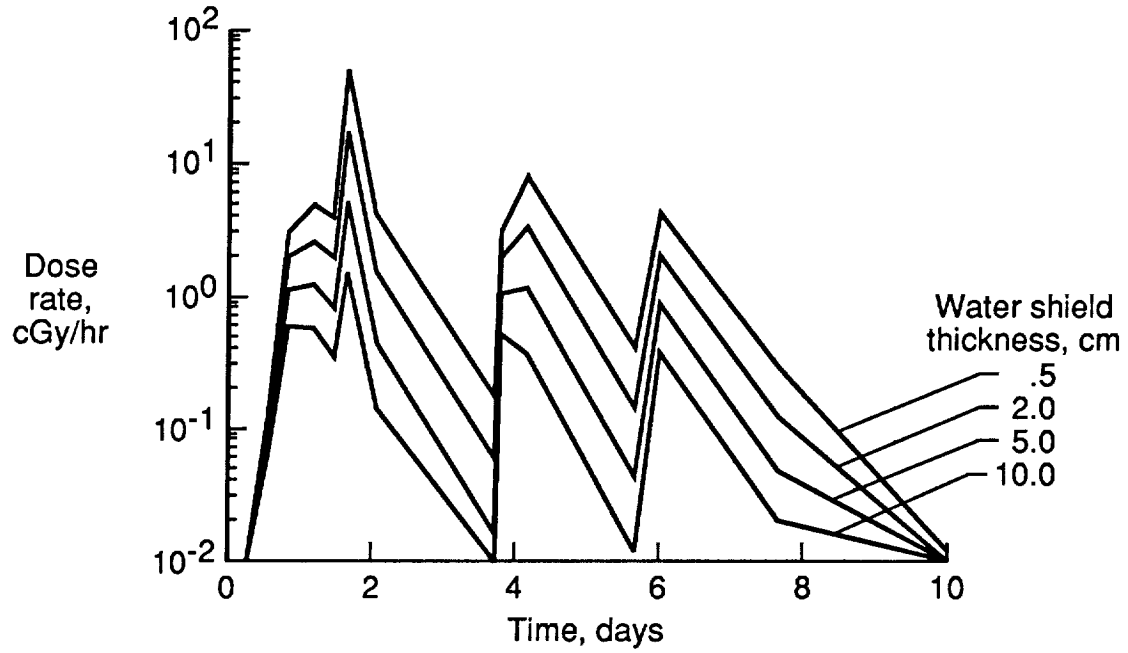

(a) Eye dose rate.

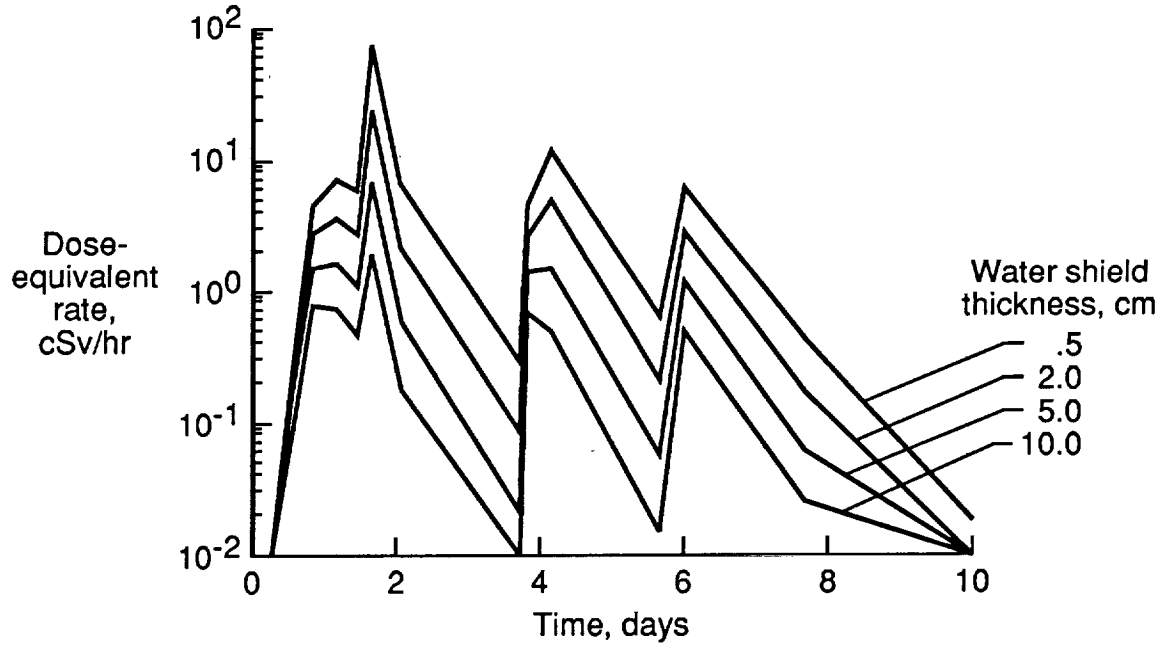

(b) Eye dose-equivalent rate.

Figure 15. Predicted eye dose rate variation and cumulative dose during October 1989 event with 0.5, 2.0, 5.0, and 10.0 cm of water shield thickness.

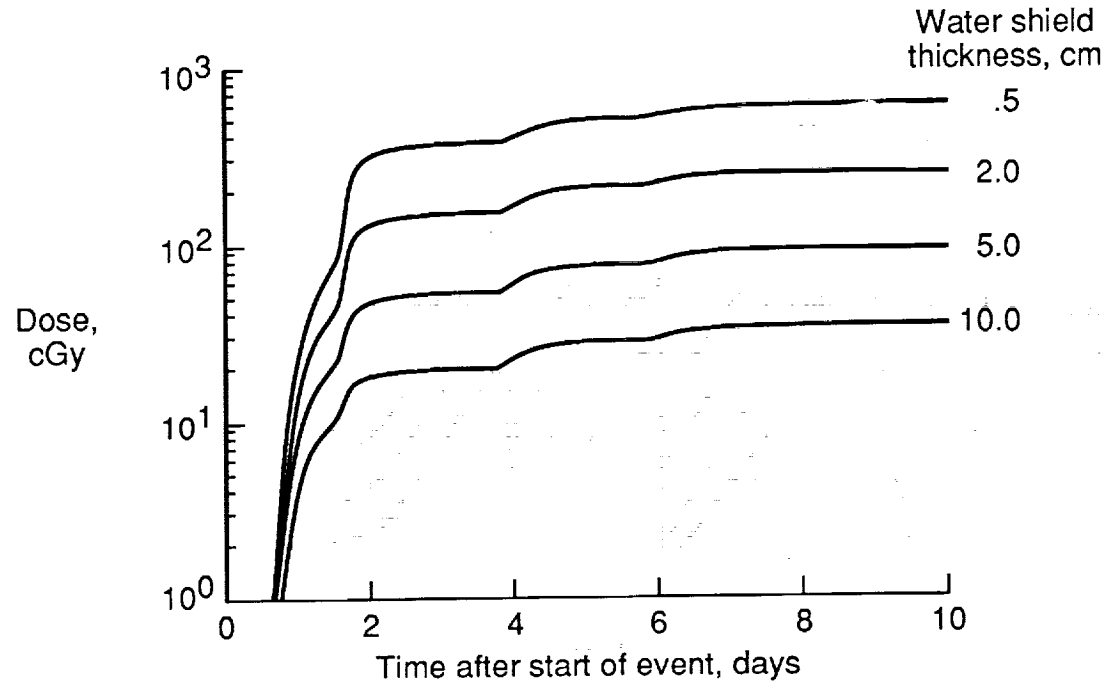

(c) Cumulative eye dose.

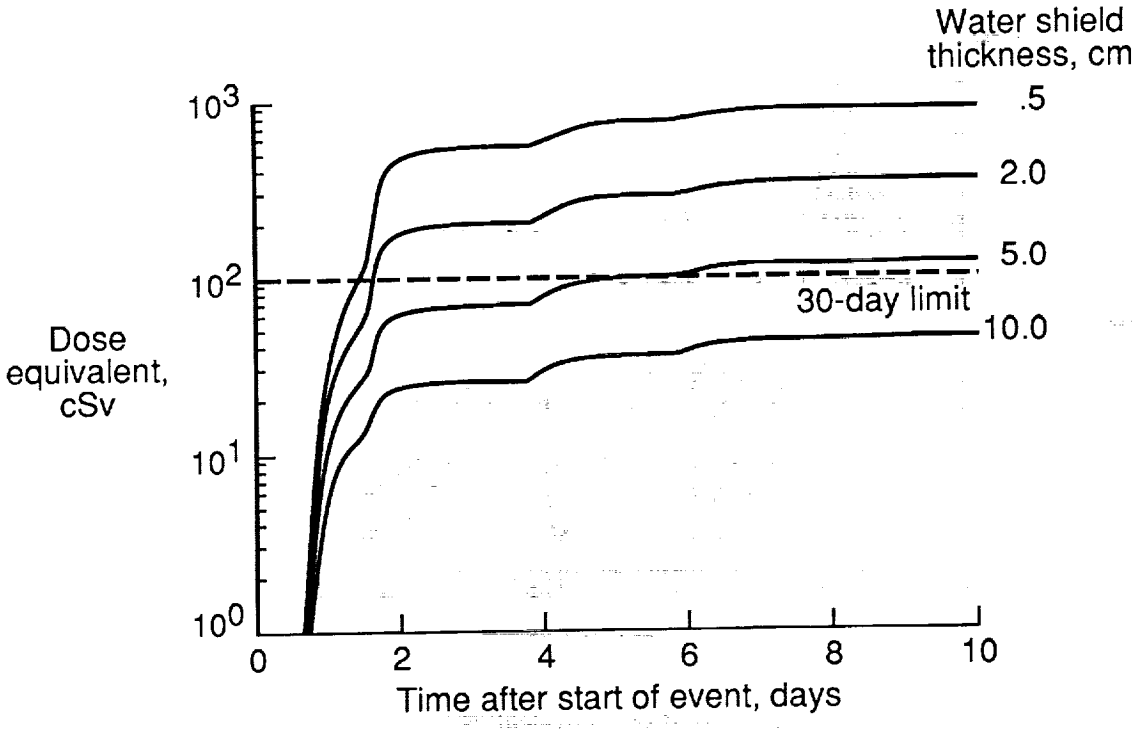

(d) Cumulative eye dose equivalent.

Figure 15. Concluded.

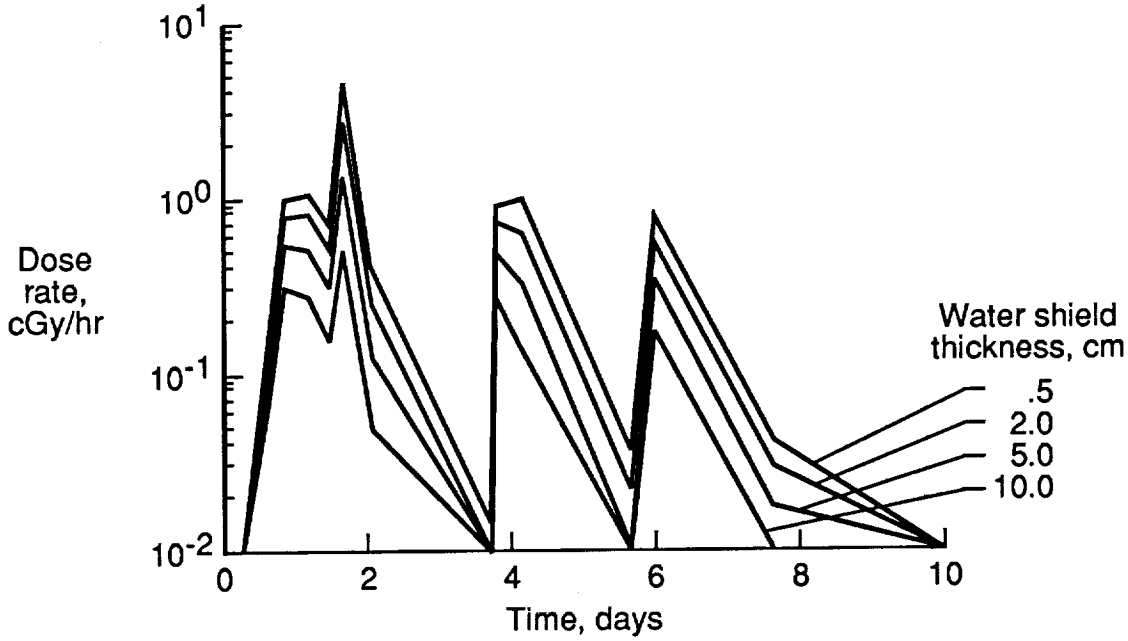

(a) BFO dose rate.

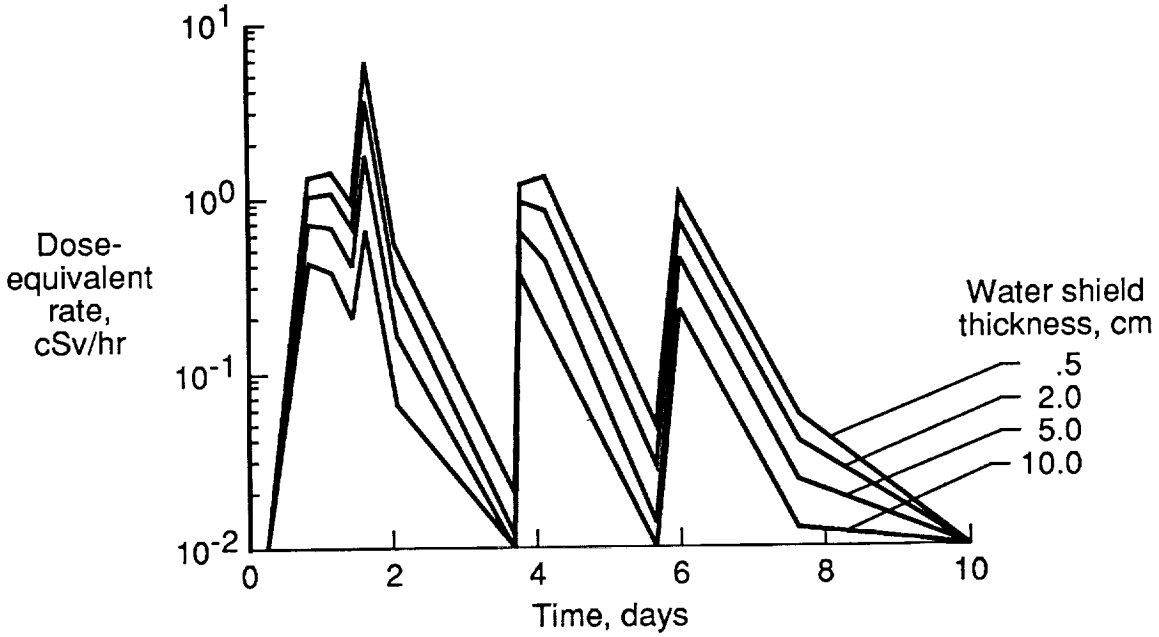

(b) BFO dose-equivalent rate.

Figure 16. Predicted BFO dose rate variation and cumulative dose during October 1989 event with 0.5, 2.0, 5.0, and 10.0 cm of water shield thickness.

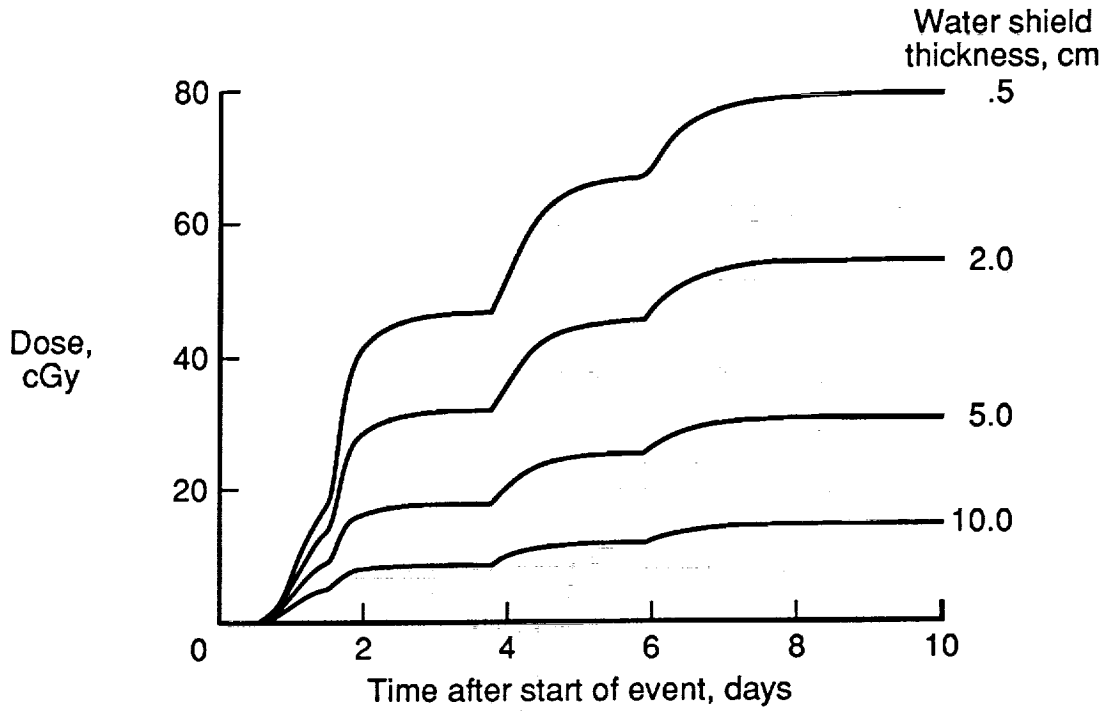

(c) Cumulative BFO dose.

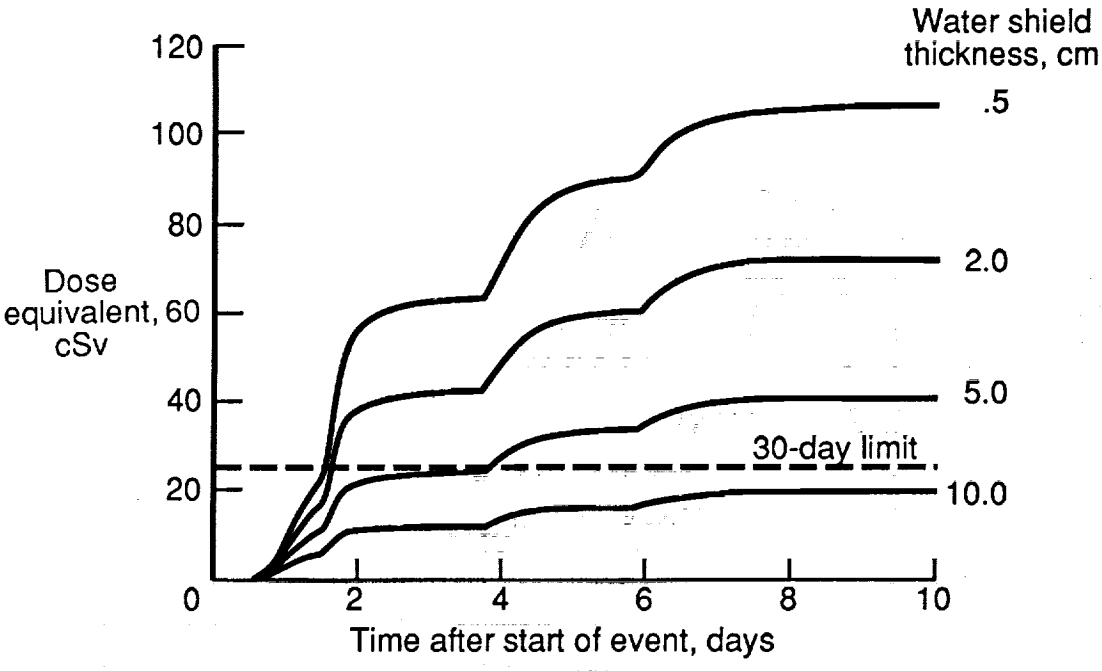

(d) Cumulative BFO dose equivalent.

Figure 16. Concluded.

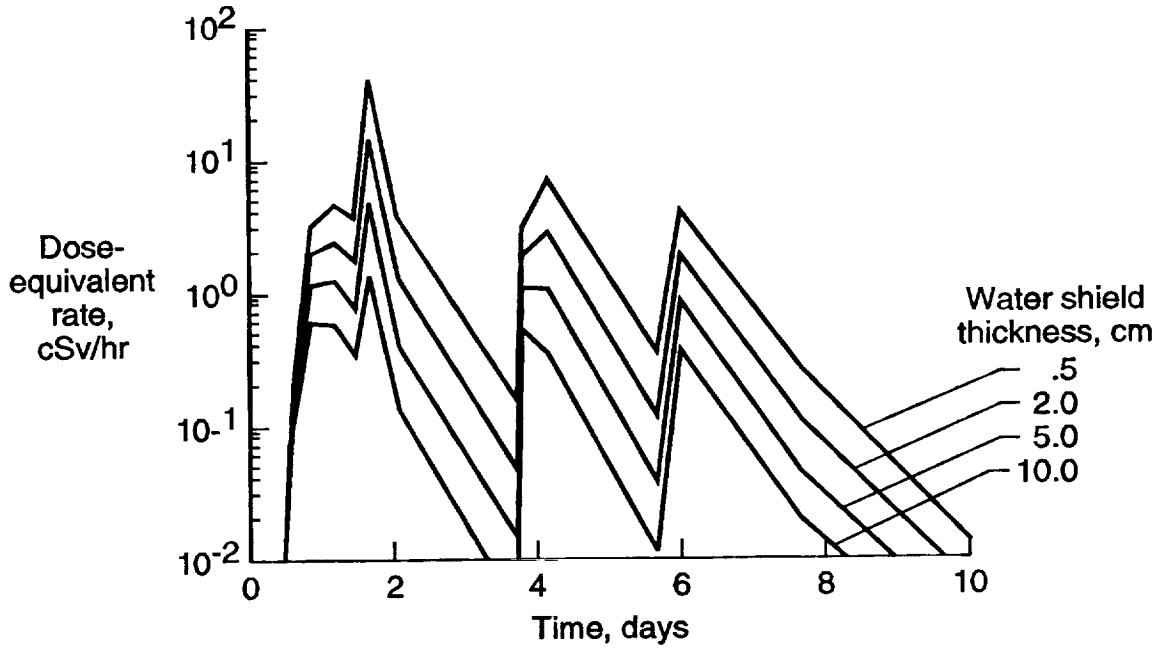

(a) Thyroid dose-equivalent rate.

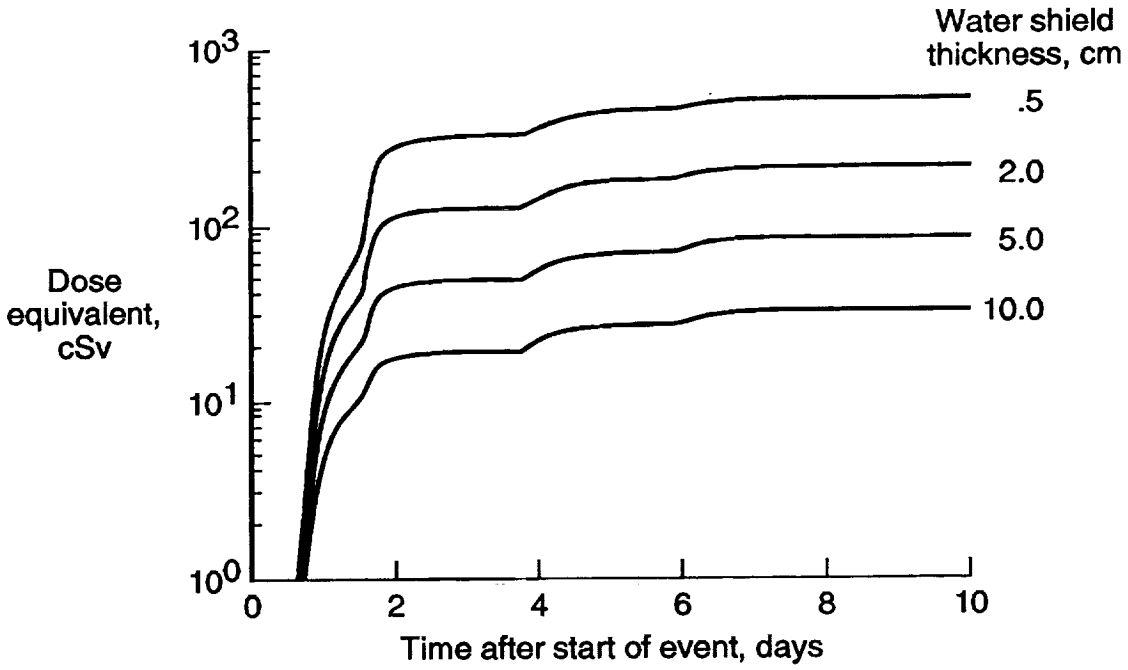

(b) Cumulative thyroid dose equivalent.

Figure 17. Predicted male thyroid dose-equivalent rate variation and cumulative dose equivalent during October 1989 event with 0.5, 2.0, 5.0, and 10.0 cm of water shield thickness.

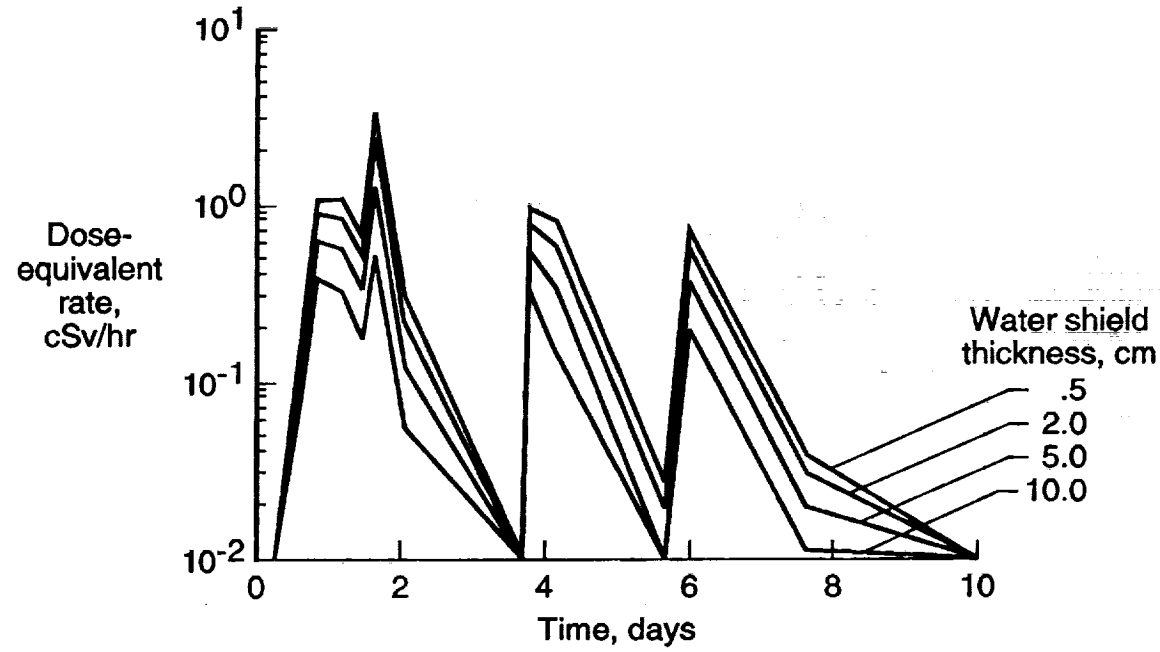

(a) Right lung dose-equivalent rate.

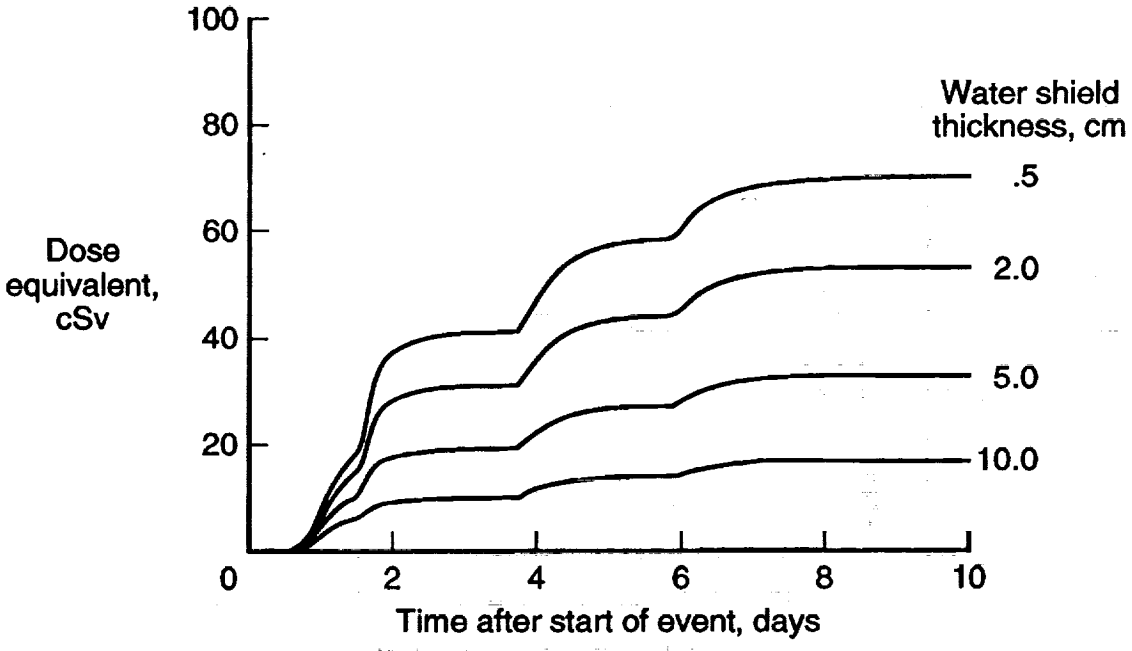

(b) Cumulative right lung dose equivalent.

Figure 18. Predicted male right lung dose-equivalent rate variation and cumulative dose equivalent during October 1989 event with 0.5, 2.0, 5.0, and 10.0 cm of water shield thickness.

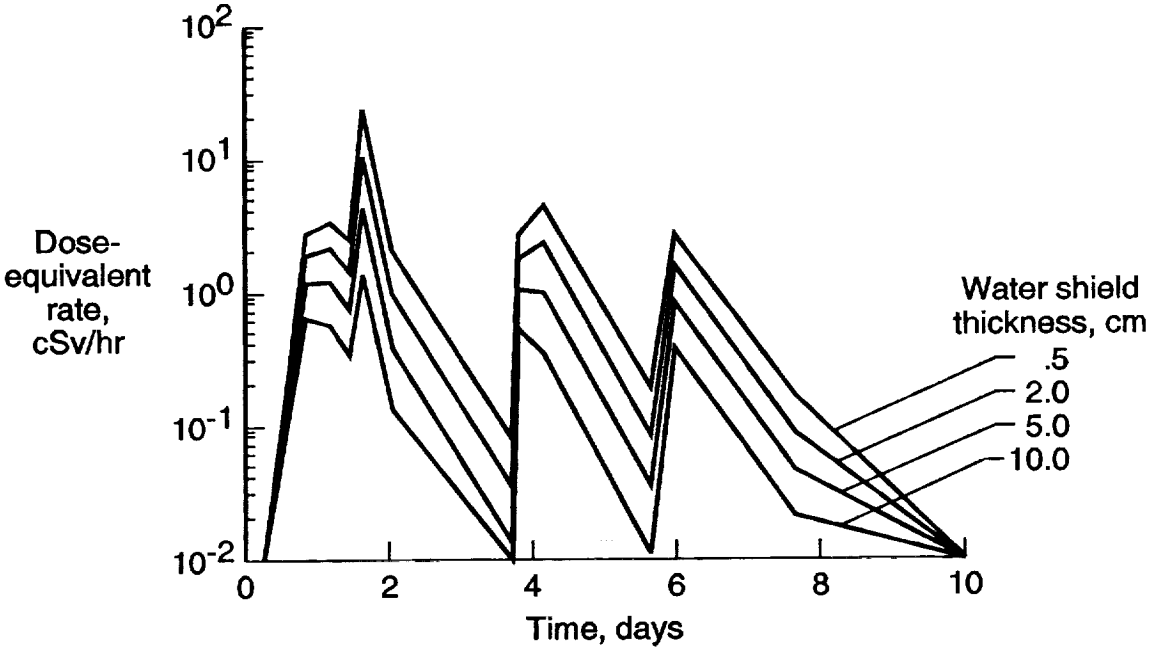

(a) Right breast dose-equivalent rate.

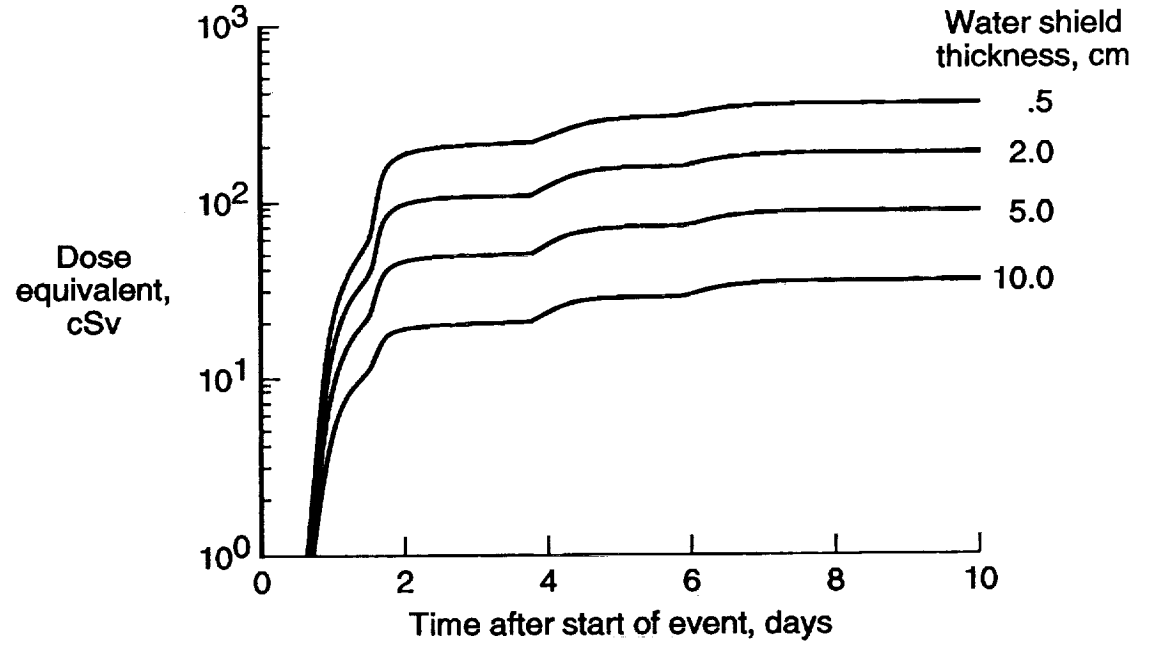

(b) Cumulative right breast dose equivalent.

Figure 19. Predicted female right breast dose-equivalent rate variation and cumulative dose equivalent during October 1989 event with 0.5, 2.0, 5.0, and 10.0 cm of water shield thickness.

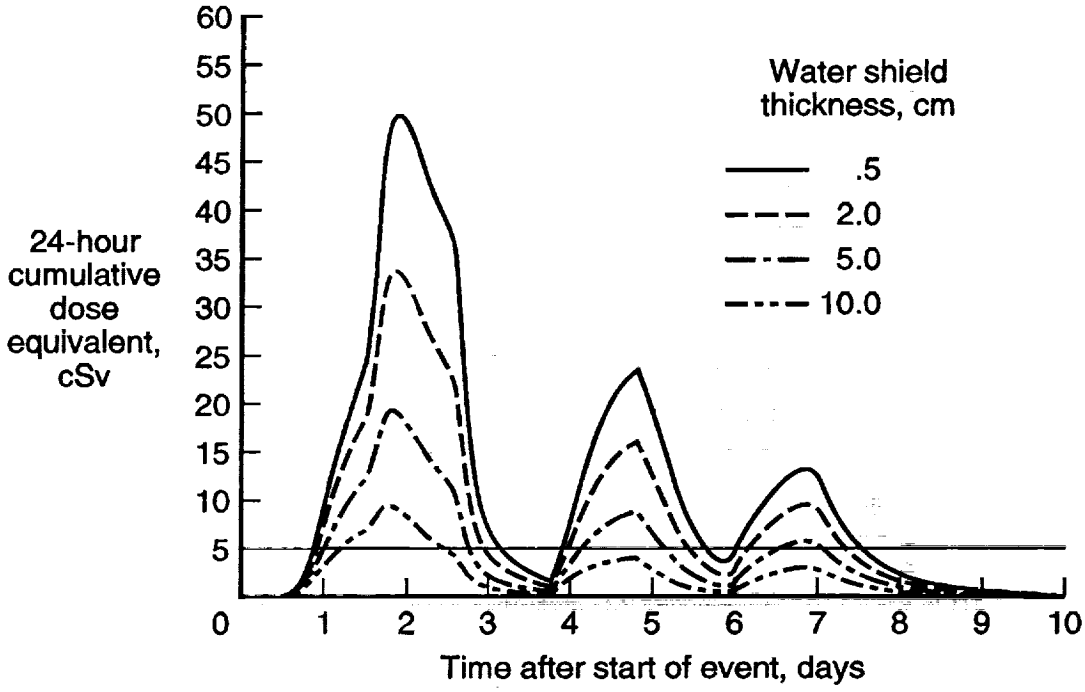

Figure 20. 24-hour cumulative dose equivalent as a function of time to BFO for October 1989 event for water shield thicknesses of 0.5, 2.0, 5.0, and 10.0 cm.

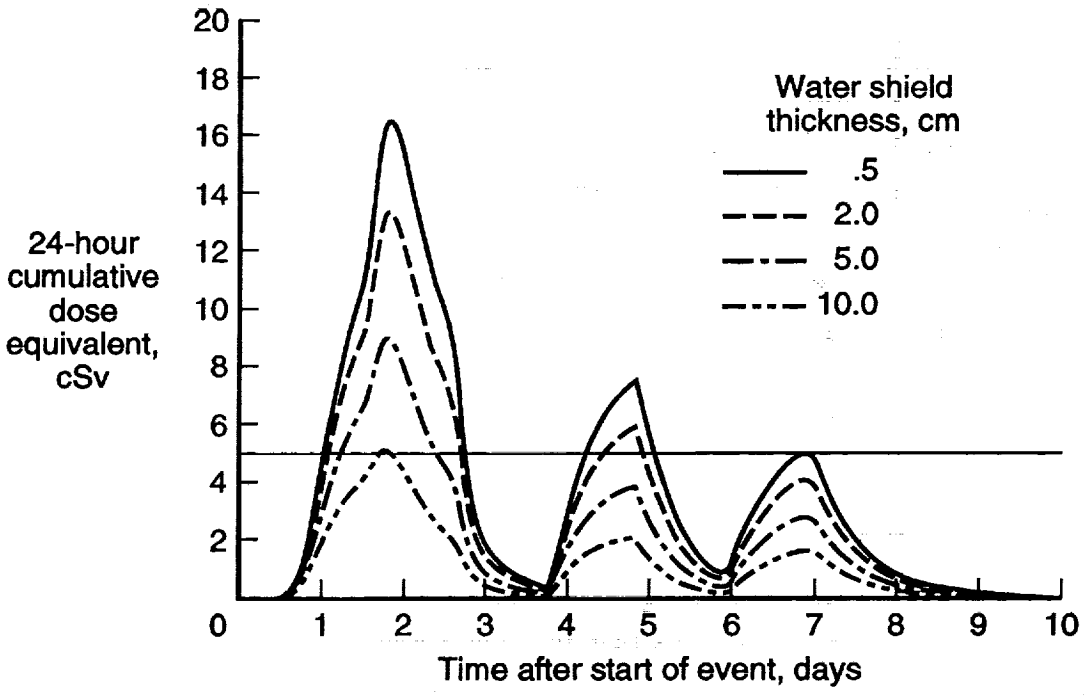

Figure 21. 24-hour cumulative dose equivalent as a function of time to stomach for October 1989 event for water shield thicknesses of 0.5, 2.0, 5.0, and 10.0 cm.

REPORT DOCUMENTATION PAGE

Form Approved
OMB No. 0704-0188

1. AGENCY USE ONLY *(Leave blank)*	2. REPORT DATE	3. REPORT TYPE AND DATES COVERED
	September 1992	Technical Paper

4. TITLE AND SUBTITLE
Radiation Dose to Critical Body Organs for October 1989 Proton Event

5. FUNDING NUMBERS
WU 593-42-31-01

6. AUTHOR(S)
Lisa C. Simonsen, William Atwell, John E. Nealy, and Francis Cucinotta

7. PERFORMING ORGANIZATION NAME(S) AND ADDRESS(ES)
NASA Langley Research Center
Hampton, VA 23681-0001

8. PERFORMING ORGANIZATION REPORT NUMBER
L-17078

9. SPONSORING/MONITORING AGENCY NAME(S) AND ADDRESS(ES)
National Aeronautics and Space Administration
Washington, DC 20546-0001

10. SPONSORING/MONITORING AGENCY REPORT NUMBER
NASA TP-3237

11. SUPPLEMENTARY NOTES
Simonsen: Langley Research Center, Hampton, VA; Atwell: Rockwell International Space Systems Division, Houston, TX; Nealy and Cucinotta: Langley Reseach Center, Hampton, VA.

12a. DISTRIBUTION/AVAILABILITY STATEMENT
Unclassified Unlimited

Subject Category 16

12b. DISTRIBUTION CODE

13. ABSTRACT *(Maximum 200 words)*

The Geostationary Operational Environmental Satellite (GOES-7) provides high-quality environmental data about the temporal development and energy characteristics of the protons emitted during a solar particle event. The GOES-7 time history of the hourly averaged integral proton flux for various particle kinetic energies are analyzed for the solar proton event occurring October 19 29, 1989. This event is similar to the August 1972 event that has been widely studied to estimate free-space and planetary radiation-protection requirements. By analyzing the time-history data, the dose rates, which can vary over many orders of magnitude in the early phases of the flare, can be estimated as well as the cumulative dose as a function of time. When basic transport results are coupled with detailed body organ thickness distributions calculated with the Computerized Anatomical Man and Computerized Anatomical Female models, the dose rates and cumulative doses to specific organs can be predicted. With these results, the risks of cancer incidence and mortality are estimated for astronauts in free space protected by various water shield thicknesses.

14. SUBJECT TERMS	15. NUMBER OF PAGES
Computerized anatomical models; October 1989 solar proton event; Radiation shielding; Dose rates; Cancer risk	33
	16. PRICE CODE A03

17. SECURITY CLASSIFICATION OF REPORT	18. SECURITY CLASSIFICATION OF THIS PAGE	19. SECURITY CLASSIFICATION OF ABSTRACT	20. LIMITATION OF ABSTRACT
Unclassified	Unclassified		